Cluster observations of traveling compression regions in the near-tail

J. A. Slavin,[1] E. I. Tanskanen,[1] M. Hesse,[1] C. J. Owen,[2] M. W. Dunlop,[3] S. Imber,[4] E. A. Lucek,[4] A. Balogh,[4] and K.-H. Glassmeier[5]

Received 14 February 2004; revised 2 November 2004; accepted 17 March 2005; published 11 June 2005.

[1] Examination of Cluster measurements has revealed the presence of traveling compression regions (TCRs) in the lobes of the Earth's magnetotail at $X \sim -11$–$19\ R_E$. These TCRs strongly resemble those observed in the more distant tail, but their mean duration is only ~35 s as compared with ~160 s for the TCRs in the distant tail. Furthermore, the B_z variations associated with the Cluster TCRs were found to be south-then-north (SN) in 80% of the cases as opposed to the north-then-south (NS) polarity that is dominant beyond $X \sim -30\ R_E$. Analysis of the time of arrival of the TCRs at the different Cluster spacecraft showed that all of the SN TCRs propagate earthward while all of the NS TCRs, as expected, move tailward. The mean speeds of the SN and NS TCRs were essentially the same, 849 km/s and 821 km/s, respectively, and their average width was $4.3\ R_E$. Some examples of near-periodic, multiple TCR events with separations between individual TCRs comparable to their width were also observed, suggestive of multiple *X*-line reconnection or periodic impulsive reconnection. However, the most probable separation observed during multi-TCR events was larger, ~100–150 s. The TCR minimum variance eigenvectors have a strong tendency to lie parallel to the GSM *XY* plane, but they exhibit a wide range of orientations within that plane. Examined as a function of the Y_{GSM}, there are broad maxima in occurrence frequency, width, and speed of TCRs on the duskside of the tail. Superposed epoch analysis of the Kyoto World Data Center Quick Look *AL* Index relative to the time of TCR occurrence shows that the compression regions tend to be observed during the expansion phase of substorms. Finally, the origins of the traveling compression regions in the near-tail are discussed in terms of the effects of magnetic flux rope motion and impulsive reconnection.

Citation: Slavin, J. A., E. I. Tanskanen, M. Hesse, C. J. Owen, M. W. Dunlop, S. Imber, E. A. Lucek, A. Balogh, and K.-H. Glassmeier (2005), Cluster observations of traveling compression regions in the near-tail, *J. Geophys. Res.*, *110*, A06207, doi:10.1029/2004JA010878.

1. Introduction

[2] Highly successful conceptual models describing the effects of magnetic reconnection on the topology of the Earth's magnetic tail were developed by *Schindler* [1974] and *Hones* [1977] nearly 3 decades ago. However, experimental confirmation has come slowly due to the limited availability of multipoint measurements. Still, even using sparse, single spacecraft (s/c) observations, many of the effects of reconnection can be readily detected. In particular, closed flux tube reconnection in the plasma sheet was predicted to produce large magnetic structures with topologies ranging from simple loops to force-free flux ropes with strong core fields [*Moldwin and Hughes*, 1991; *Birn et al.*, 1989; *Hughes and Sibeck*, 1987]. These structures, termed "plasmoids" by *Hones* [1977], were first definitively observed in the ISEE 3 [*Moldwin and Hughes*, 1992; *Slavin et al.*, 1989; *Baker et al.*, 1987; *Richardson et al.*, 1987; *Hones et al.*, 1984] and Geotail [*Machida et al.*, 2000; *Ieda et al.*, 1998; *Mukai et al.*, 1998, 1996; *Nagai et al.*, 1994] distant tail measurements where they were observed to have typical dimensions of ~10–30 R_E and to move tailward at ~600–800 km/s following the onset of substorms.

[3] The interaction of these large, fast-moving flux ropes with the lobes of the distant tail produced another readily observable phenomenon, the traveling compression region or "TCR" [*Slavin et al.*, 1984]. The tension of the magnetic field lines in nascent flux ropes cause them to become progressively more cylindrical by shrinking in the $\pm X$ and growing in the $\pm Z$ directions. This produces a bulge in the thickness of the plasma sheet that compresses the lobes. When the flux rope is carried earthward or tailward by fast flow emanating from a near-Earth neutral line (NENL), the lobe compression "travels" with the flux rope. TCRs have been studied extensively in the deep tail measurements and have played a significant role in establishing the central role

[1]Laboratory for Extraterrestrial Physics, NASA Goddard Space Flight Center, Greenbelt, Maryland, USA.
[2]Mullard Space Science Laboratory, University College London, Surrey, UK.
[3]Rutherford Appleton Laboratory, Oxfordshire, UK.
[4]Space and Atmospheric Physics, Imperial College, London, UK.
[5]Institut für Geophysik und extraterrestrische Physik, Technische Universität Braunschweig, Braunschweig, Germany.

0148-0227/05/2004JA010878$09.00

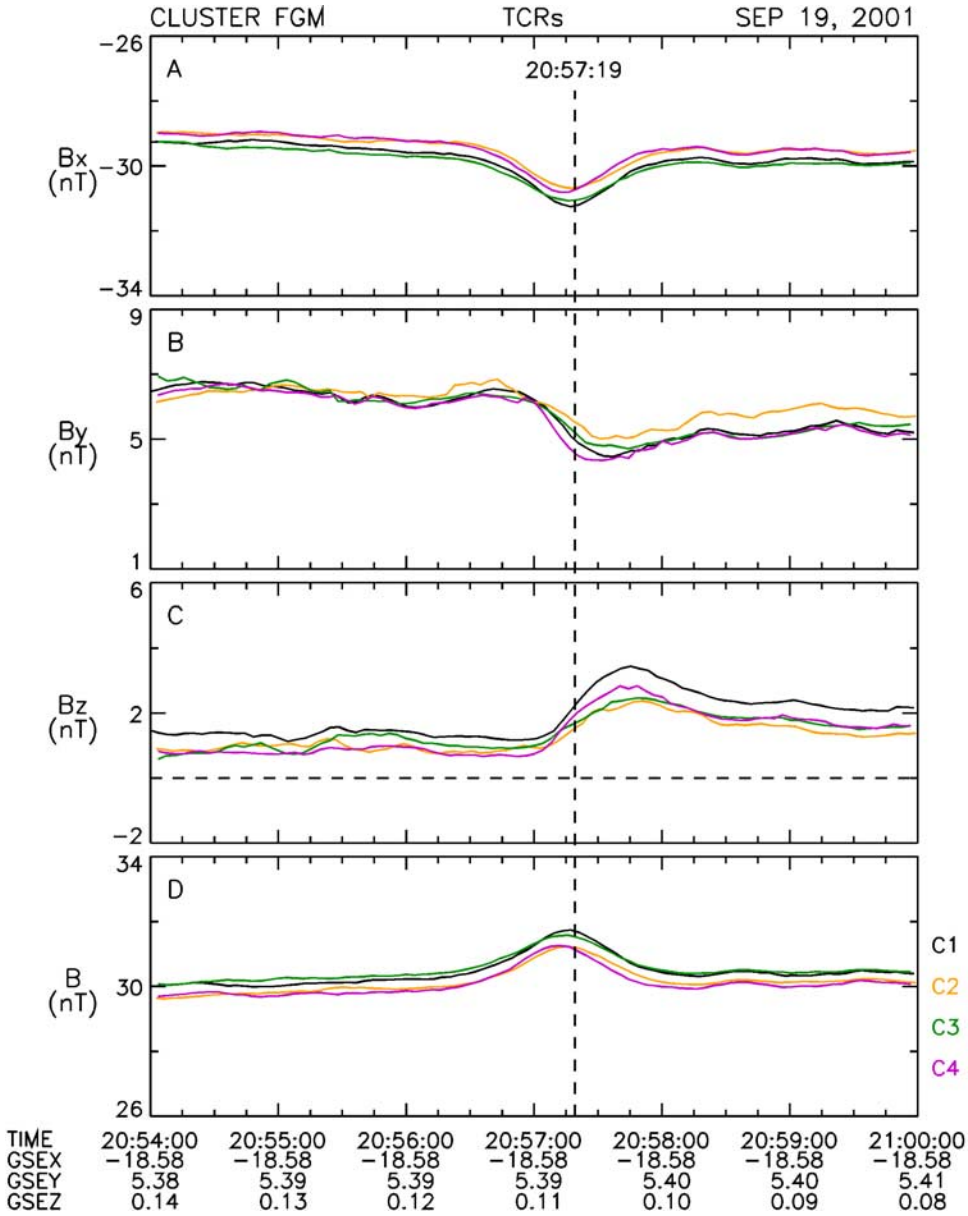

Figure 1. An example of an earthward moving traveling compression region in the Cluster fluxgate magnetometer (FGM) measurements on 19 September 2001.

of reconnection in the substorm process [*Huang et al.*, 2003; *Slavin et al.*, 2002, 1998, 1993, 1992; *Shirai et al.*, 2001; *Taguchi et al.*, 1998, 1997; *Owen and Slavin*, 1992].

[4] Recently, *Slavin et al.* [2003c], *Owen et al.* [2005], and V. A. Sergeev et al. (submitted manuscript, 2005) have reported the first observations of TCRs at $X > -20\ R_E$ in the Cluster measurements. An example of such a TCR in the Cluster measurements is shown in Figure 1. *Slavin et al.* [2003c] found that these brief compressions of the lobe field were accompanied by the familiar $\pm\Delta B_z$ perturbations observed in the distant tail. The durations of these TCRs were typically only a few tens of seconds as contrasted with $\sim$1–3 min in the distant tail [*Slavin et al.*, 1993]. It was suggested by *Slavin et al.* [2003c] that the brief duration of the Cluster TCRs is consistent with their being caused by the rapid motion of the small flux ropes embedded in the near-Earth plasma sheet also recently discovered in the Geotail [*Slavin et al.*, 2003a] and Cluster measurements [*Zong et al.*, 2004; *Slavin et al.*, 2003b]. However, as with flux transfer events (FTEs) at the dayside magnetopause [*Sonnerup et al.*, 2004; *Russell and Elphic*, 1978], these near-tail TCRs could also be produced by highly time-dependent, "impulsive" reconnection as suggested by *Sergeev et al.* [1992, 1987, submitted manuscript, 2005].

[5] Here we present a comprehensive analysis of the Cluster TCR observations collected during the 2001 and 2002 tail seasons. These four s/c observations are used to determine the direction and speed of propagation of the TCRs and to derive other properties such as their orientation and spatial scales. The relative occurrence of earthward and tailward moving TCRs is used to assess the frequency with which neutral lines form earthward of the Cluster apogee at $X \sim -20\ R_E$ and their substorm association is examined using the Kyoto World Data Center Quick Look *AL* Index.

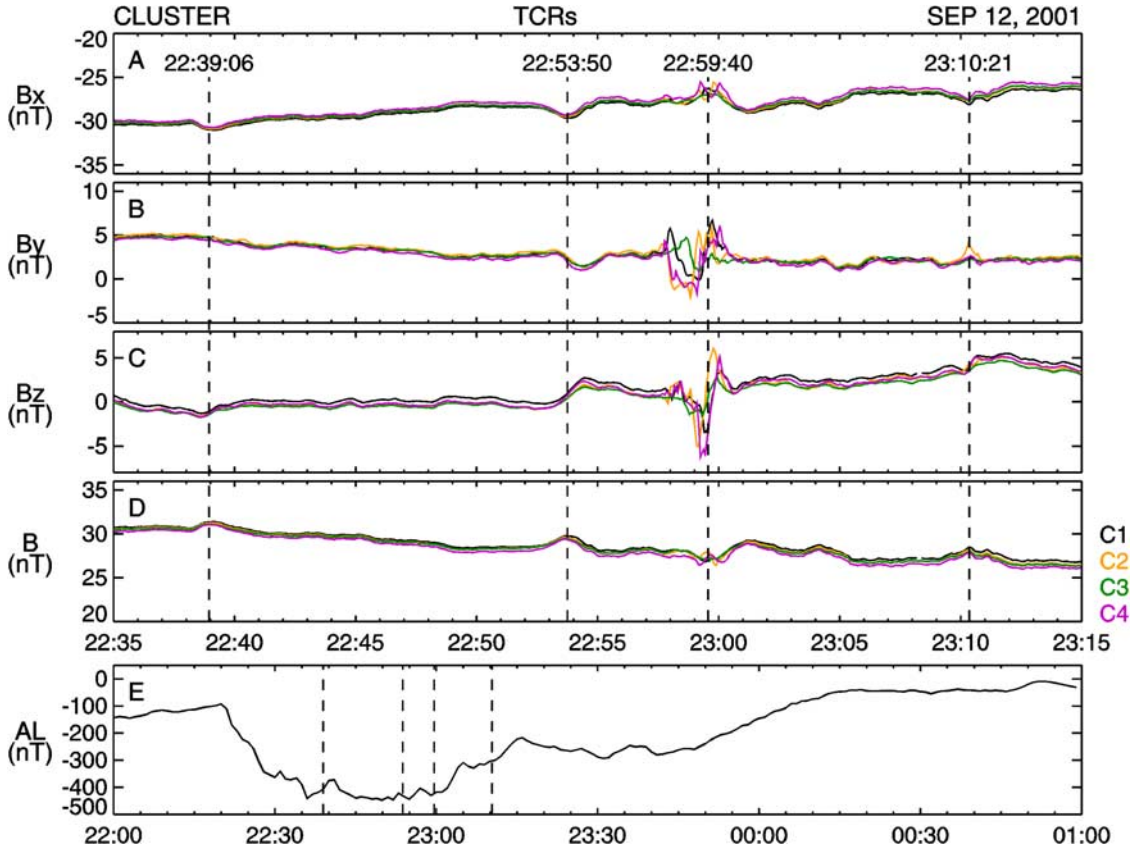

Figure 2. An example of traveling compression regions in the Cluster FGM measurements on 12 September 2001. A total of four south-to-north (SN) traveling compression regions (TCRs) are marked with vertical lines albeit the third event from the left occurs in the boundary layer between the lobe and plasma sheet as evidenced by the small compression and large $\pm B_z$ perturbation.

Finally, the properties of the TCRs determined here are discussed in terms of their likely generation mechanisms.

2. Cluster TCR Survey and Superposed Epoch Analysis

[6] Each year between August and October the Cluster spacecraft apogee lies within the tail. For the purposes of surveying TCR frequency of occurrence, spatial distribution, and physical properties we scanned spin period, i.e., ~4 s, resolution Cluster fluxgate magnetometer (FGM) measurements [*Balogh et al.*, 1997] to identify all TCRs with durations between a few seconds and several minutes and compression ratios, $\Delta B/B$, greater than ~1%.

[7] Figure 2 shows an example of Cluster magnetic field measurements collected during a 40-min interval on 12 September 2001 during the expansion and early recovery phases of a substorm identified using the Kyoto Quick-look *AL* index (http://swdcwww.kugi.kyoto-u.ac.jp/aedir/index.html). A total of four TCRs were identified and marked with vertical dashed lines. We required distinct, well correlated B_x and B_z perturbations for event identification but not at all four s/c. While it was generally the case that all of the s/c remained in the lobes and the magnetic field perturbations at the four s/c differed primarily by a simple time shift of a few seconds, sometimes one or two s/c, especially s/c 3 that forms the southern vertex of the tetrahedral formation, would pass into the bulge in the plasma sheet generating the TCR. The third TCR from the left in Figure 2 provides an example of such case where most of the spacecraft penetrated in the outer layers of the plasma sheet. For each of the s/c that encountered the plasma sheet, an increase in the amplitude of the B_z perturbation and a reduction in the magnetic field compression signal is observed. *Slavin et al.* [2003c] used such events to determine a ~1 R_E amplitude for the plasma sheet bulges causing the compression regions in their initial study of TCRs in the very near-tail.

[8] A total of 148 TCRs were identified during the 2001 and 2002 Cluster tail seasons. The locations of the TCRs are projected into the GSM *X-Y* and *X-Z* planes are shown in Figure 3a. The TCRs with north-then-southward (NS) ΔB_z events are plotted with red triangles while the southward-then-northward (SN) ΔB_z events appear as black dots. Of the 119 total, 80% were of the SN type and presumably moving earthward, while the remaining 29, or 20%, were tailward moving NS TCRs. Spatially, the distribution of the SN and NS TCRs at Cluster were very similar with most occurring within ± 10 R_E of the *X* axis and tailward of $X \sim -12$ R_E. The only notable asymmetry in TCR location is that more events are seen in the dusk as opposed the dawnside of the tail. For each tail season we estimated that Cluster spent about 120,000 min in lobe regions beyond $X \sim -12$ R_E for a total of 240,000 min or 4000 hours

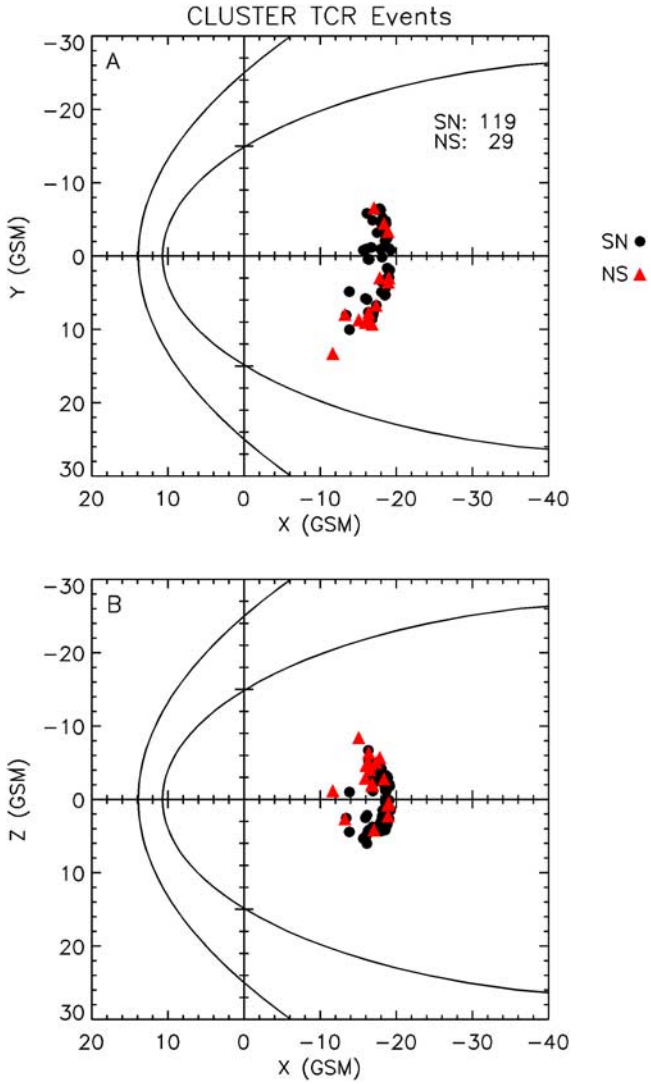

Figure 3a. The locations of the 119 SN and 29 north-to-south (NS) TCRs are marked with black circles and red triangles, respectively. These events were identified in identified in the 2001 and 2002 Cluster FGM observations.

over the 2 years. The calculated average frequency of occurrence of compression regions in the Cluster data is about 1 TCR per 27 hours or about 1 per day.

[9] TCR measurements have been used to conduct superposed epoch analyses of the two types of events with a ±120 s window. Figures 3b and 3c display the results for the SN and NS TCRs, respectively. In both cases the zero epoch is taken to be the center of the TCR perturbation at s/c 1. The top two parts of both figures display the absolute values of B_x and B_y so that events in both the north and south lobes and the dawnside and duskside of the tail can be combined. The lower two parts of Figures 3b and 3c show B_z and B magnitude.

[10] The widths of the SN and NS TCRs based upon the extremes in B_z are very similar with mean durations based upon the extremes in the B_z perturbation of ~36 s. The B_y signatures in both figures are small relative to the other components. Close inspection of the magnetic field traces also show that for the SN TCRs the perturbation is first seen at s/c 4 and, a few seconds later, at s/c 1 consistent with earthward propagation because s/c 1 and s/c 4 were located near the Sun–Earth line with separations in X_{GSM} of several thousand kilometers, The opposite ordering is seen for the NS TCRs indicating the expected tailward propagation. Furthermore, the mean compression ratios, $\Delta B/B$, for both types of TCR are similar at ~4%.

[11] However, the SN and NS TCRs differ markedly in the strength of the lobe field typical of each. The SN TCRs are observed when the mean lobe is ~27 nT while the NS events occurred during a mean lobe magnetic field of ~32 nT or about 16% greater than for the SN TCRs. As shown in Figure 3b, the SN TCRs are seen in a closed field region of the tail where B_z is positive everywhere and becomes still more positive as additional magnetic flux is closed tailward of the TCR by continued lobe flux tube reconnection. Figure 3c presents the mirror image case for the tailward propagating TCRs. These NS events are observed in a region of the tail that is disconnected from the Earth in terms of its magnetic topology. As shown, B_z is negative everywhere and becomes more negative following the passage of the TCR as additional flux tubes are disconnected by continued reconnection between the lobes.

3. TCR Propagation Velocity

[12] Cluster magnetic field measurements allow the direction and propagation speed, V_n, of the TCRs to be determined using "triangularization." Although the Cluster spacecraft all take slightly different paths through the compression region, they will record similar magnitude profiles with the peak marking the center line of the plasma sheet bulge and the surrounding compression region. Lag correlations can then be performed between the compression signatures at pairs of spacecraft and propagation times determined. With the assumption that the TCR compression can be approximated as a plane discontinuity, or wave front, the delays between two pair of spacecraft may be used to determine the speed, V_n, and direction of propagation in the GSM X-Y plane. Since the TCRs propagate predominantly in the X-Y plane, the time delays in the Z direction are usually very small, which results in large uncertainties. For this reason, the TCR propagation velocity determination was limited to the GSM X-Y plane.

[13] Specifically, we take the time delay for propagation from s/c j to s/c i to be T_{ij}. Similarly, the components of the separation vector from s/c j to s/c i are R_{ijx} and R_{ijy}. The angle, α, that the TCR compression front makes to the Sun–Earth axis is

$$\alpha = \arctan(A), \tag{1}$$

where

$$A = \left[R_{24y}T_{14} - R_{14y}T_{24}\right]/\left[R_{14x}T_{24} - R_{24x}T_{14}\right]. \tag{2}$$

The speed of the TCR, presumably normal to the long axis of the underlying bulge in the plasma sheet is then just

$$V_n = \left[R_{14x}/T_{14}\right]\sin(\alpha), \tag{3}$$

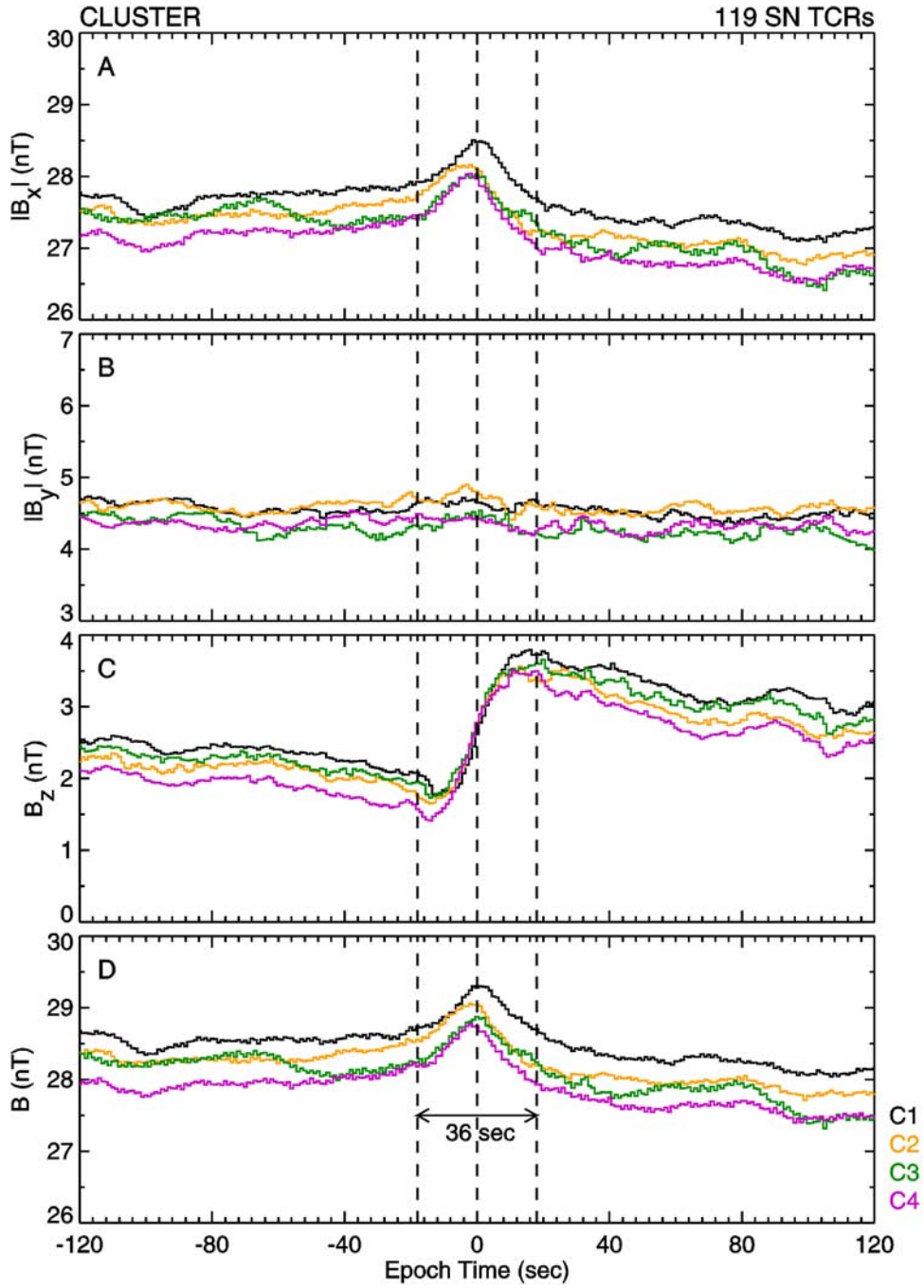

Figure 3b. Superposed epoch analysis of the 119 SN TCRs over a window of ±120 s with the zero epoch corresponding to the center of the magnetic perturbation at s/c 1. Vertical dashed lines indicate the zero epoch corresponding to the peak compression at s/c 1 and the ±18 s duration of the event. Note that TCR perturbation is first seen at the most tailward spacecraft, s/c 4 (red), and then a few seconds later at the most earthward, s/c 1 (black), consistent with sunward propagation.

with components

$$V_x = V_n \sin(\alpha) \text{ for } \alpha > 0 \quad (4)$$

$$V_x = -V_n \sin(\alpha) \text{ for } \alpha < 0 \quad (5)$$

and

$$V_y = V_n \cos(\alpha). \quad (6)$$

[14] Figures 4a presents an example of the triangularization analysis to determine TCR propagation velocity in the GSM *X*-*Y* plane. The Cluster magnetic field measurements

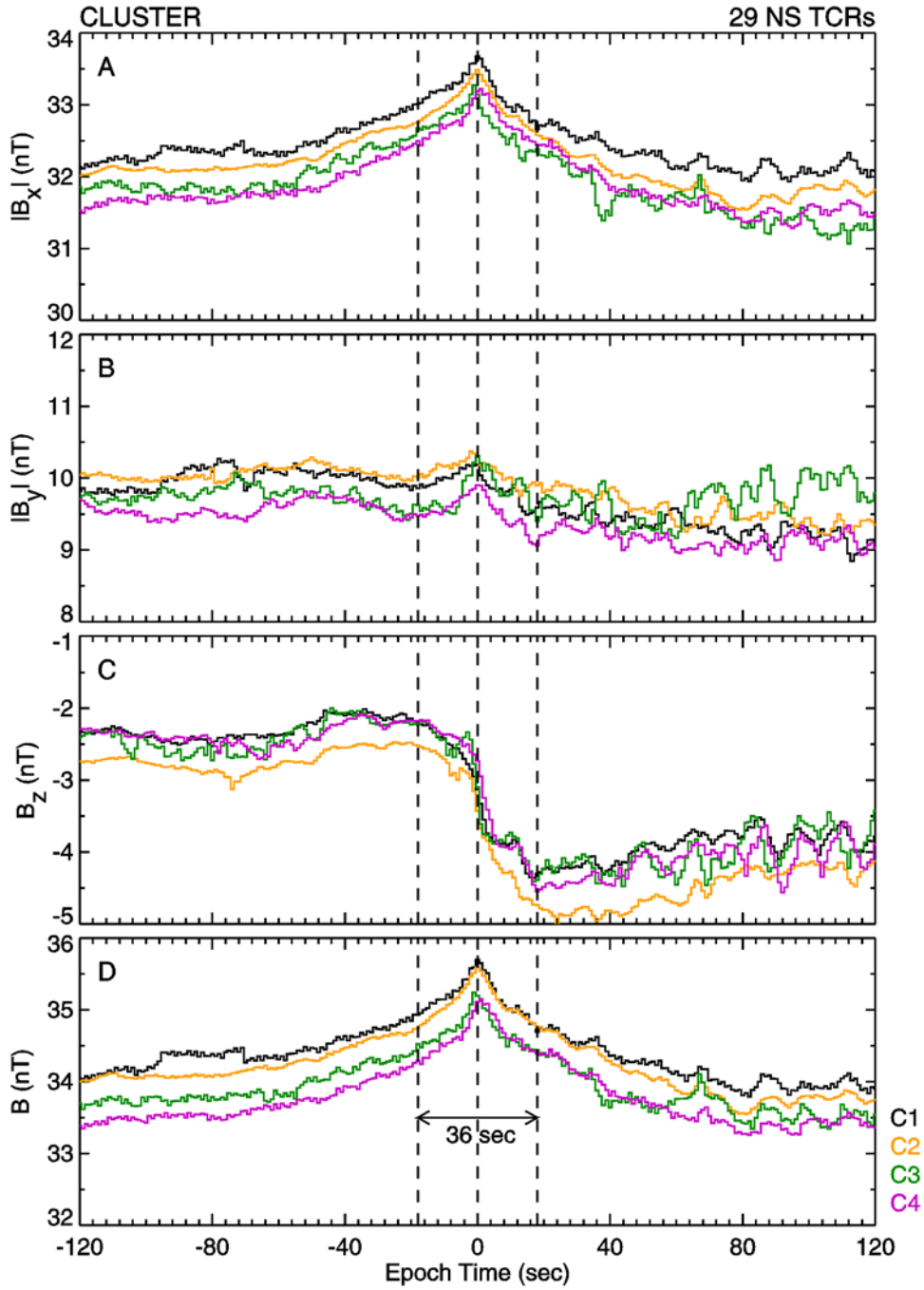

Figure 3c. Superposed epoch analysis of the 29 NS TCRs over a window of ±120 s with the zero epoch corresponding to the center of the magnetic perturbation at s/c 1. Vertical dashed lines indicate the zero epoch corresponding to the peak compression at s/c 1 and the ±18 s duration of the event. Note that TCR perturbation is first seen at the most earthward spacecraft, s/c 1 (black), and then a few seconds later at the most tailward, s/c 4 (red), consistent with anti-sunward propagation.

across a SN TCR observed at 1155:56 UT on 10 September 2001 is shown on the left side of the figure. As in the previous example, the characteristic compression and draping signatures in B_x and B_z, respectively, are present. The duration of this TCR is relatively long at 75 s based upon the extremes in the B_z perturbation and the $\Delta B/B$ is 2%. The parts to the right show the lag correlations between s/c 1–4 (top) and s/c 2–4 (bottom). In each case the correlation coefficients are excellent with peak values in excess of 0.95. The results indicate that this TCR was observed at s/c 4 before s/c 1 and 2 by 3.2 and 1.4 s, respectively. The corresponding TCR velocity is V_x = 564 km/s, V_y = −106 km/s, and the total speed is V_n = 574 km/s.

[15] We determined two-dimensional propagation velocities for 124 of the 148 TCRs identified in this study. The reasons for the failure to obtain velocities in 24 cases was

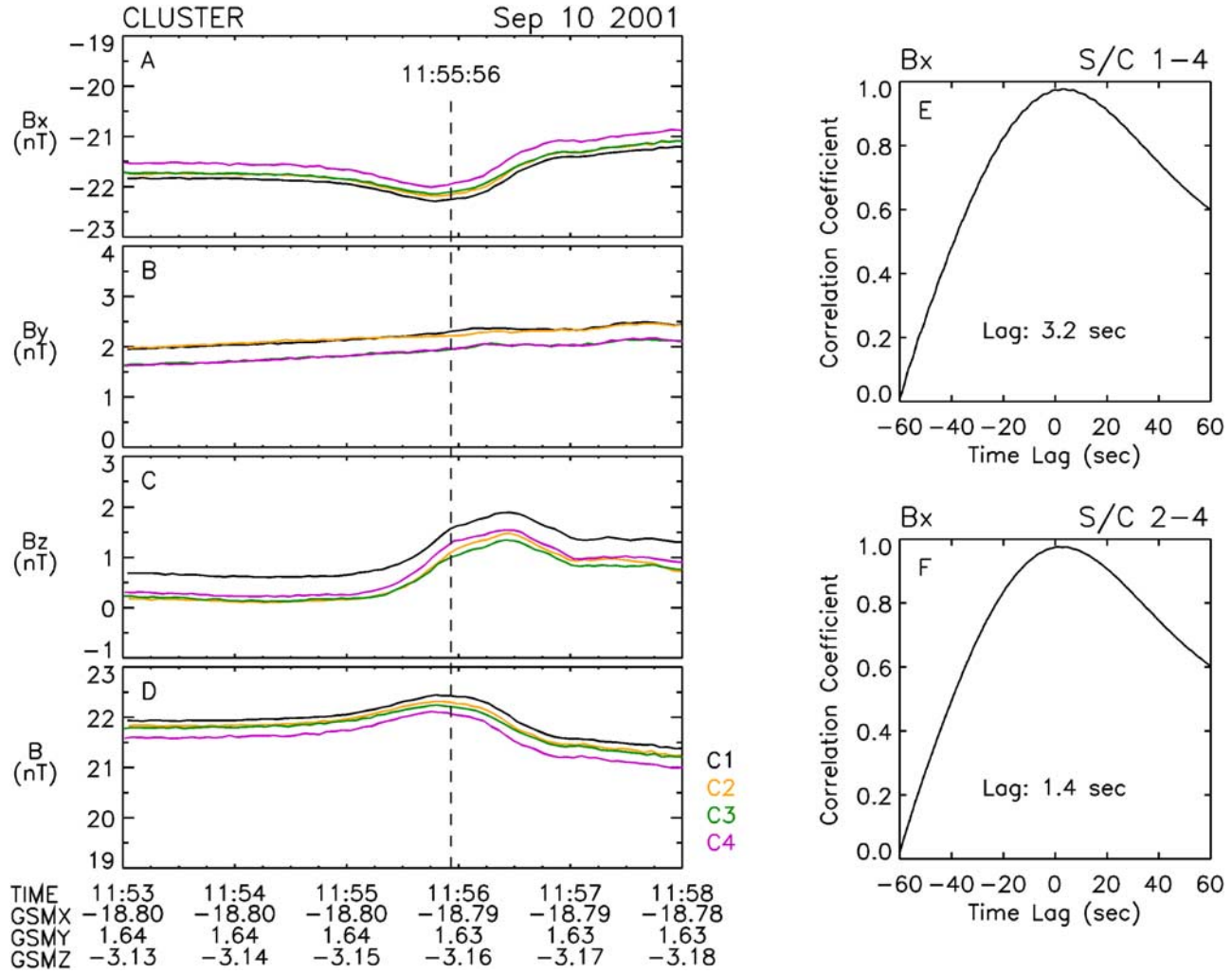

Figure 4a. Example of a SN TCR observed on 10 September 2001. Lag correlations between s/c 1 and 4 and s/c 2 and 4 are shown at the right. Triangularization yields V_x = 564 km/s and V_y = −106 km/s.

either that (1) one or more of s/c 1, 2, or 4 passed into the plasma sheet and failed to observe the TCR, (2) the cross-correlation analyses produced poor results in the sense that the peak correlation coefficient was <0.7, or (3) the TCR total velocity exceeded 2000 km/s. For TCR speeds above 2000 km/s the uncertainties in the time lags from one s/c to the next begin to produce large errors in the propagation velocity.

[16] Figure 4b displays histograms of V_x, V_y, V_n and the direction of propagation relative to the X axis, $\arctan(V_y/|V_x|)$, for the SN and NS TCRs. As shown in the top part, the V_x polarities were all consistent with the expectations based upon the sense of the B_z signature; i.e., SN and NS TCRs move earthward and tailward, respectively. The V_y speeds were centered near zero with standard deviations (SD) of ∼500 km/s. The direction of TCR propagation for the TCRs was centered very near the X axis with standard deviations of just under 30 degrees. Accordingly, the ratio of V_x to V_y is usually greater than 2 to 1. Finally, the mean propagation speeds, V_n, for the SN and NS TCRs were very similar at 849 and 821 km/s, respectively. These speeds are also typical of earthward bursty bulk flows (BBFs) [*Nagai et al.*, 2000, 1998] and tailward flow associated with plasmoids in the more distant tail [*Ieda et al.*, 2001].

[17] Using the individual TCR speeds and durations, we have also computed a width, L, for each of the events, the product of the duration and the total speed, V_n. As shown in Figure 5a the mean values, μ, for TCR duration, propagation speed, and width of 35 s, 843 km/s, and 4.3 R_E are determined. Figure 5b displays a histogram of TCR width, compression ratio, $\Delta B/B$, V_n, and numbers of TCR events as a function of the GSM Y location of s/c 1. The distribution of TCRs is strongly biased toward the duskside of the tail with 36 events being observed for $Y < 0$ and 88 for $Y > 0$. In addition, the dawnside events appear to be smaller in terms of L and the TCR speed was greater on the duskside at ∼900 as opposed to ∼700 km/s.

4. TCR Minimum Variance Analysis

[18] Insight into the orientation of TCRs can be gained from determining the principal axes of the magnetic field perturbation [*Sonnerup and Cahill*, 1967]. The $B1$ axis is defined to be along the direction of maximum variance for the magnetic field during the time interval of interest. The

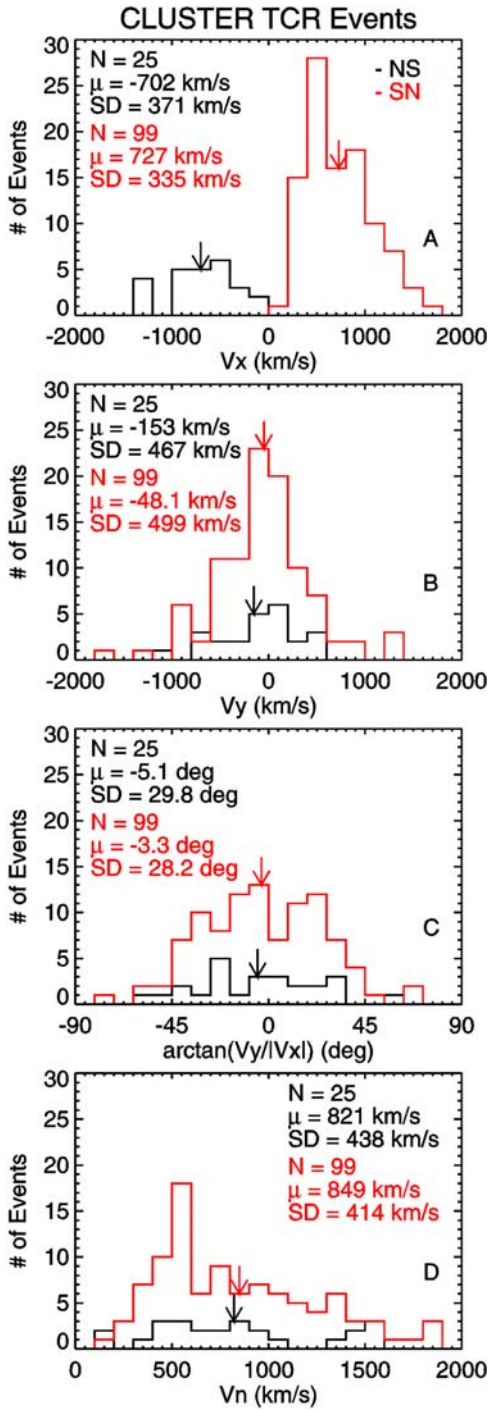

Figure 4b. Histograms of SN TCR propagation velocity components V_x, V_y, the angle that velocity makes to the X axis, arctan($V_y/|V_x|$), and the total speed, V_n, for the NS (black) and SN (red) TCRs.

other two axes, $B2$ and $B3$, are oriented along the intermediate and minimum variance directions, respectively. Minimum variance analysis has previously been applied to TCRs in the deep tail by a number of studies [*Slavin et al.*, 1993, 1984]. In general such analysis is very well suited to TCRs and it produces well defined eigenvectors with very good, i.e., large, eigenvalue ratios. The results from the more distant tail showed that the minimum axis direction was largely parallel to the Y direction and the maximum and intermediate directions were near the XZ plane [see *Slavin et al.*, 1993].

[19] In Figure 6, we show the minimum variance directions determined for all 124 of the TCRs in our study for which well-defined V_n propagation speeds could be determined. Although not shown, the magnetic field variations in principal axes coordinates displayed the expected simple half circular rotation in the $B1$-$B2$ plane and small $B3$ component with relatively large eignenvalue ratios, as found in the deep tail studies [e.g., *Slavin et al.*, 1984, 1993]. The

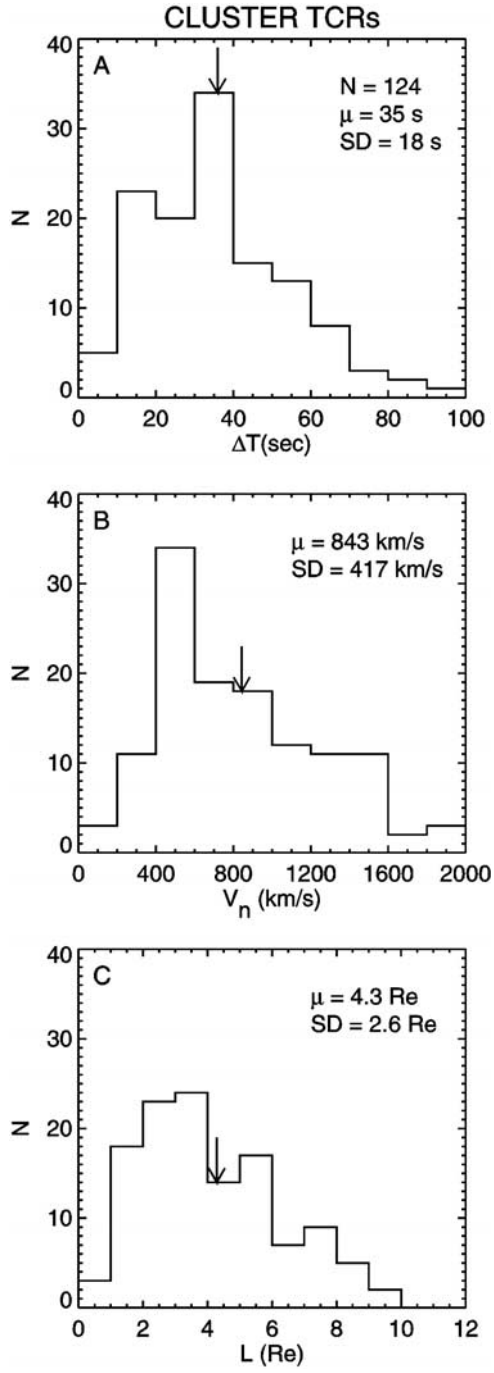

Figure 5a. Histograms of the duration, propagation speed and thickness for both the SN and NS TCRs.

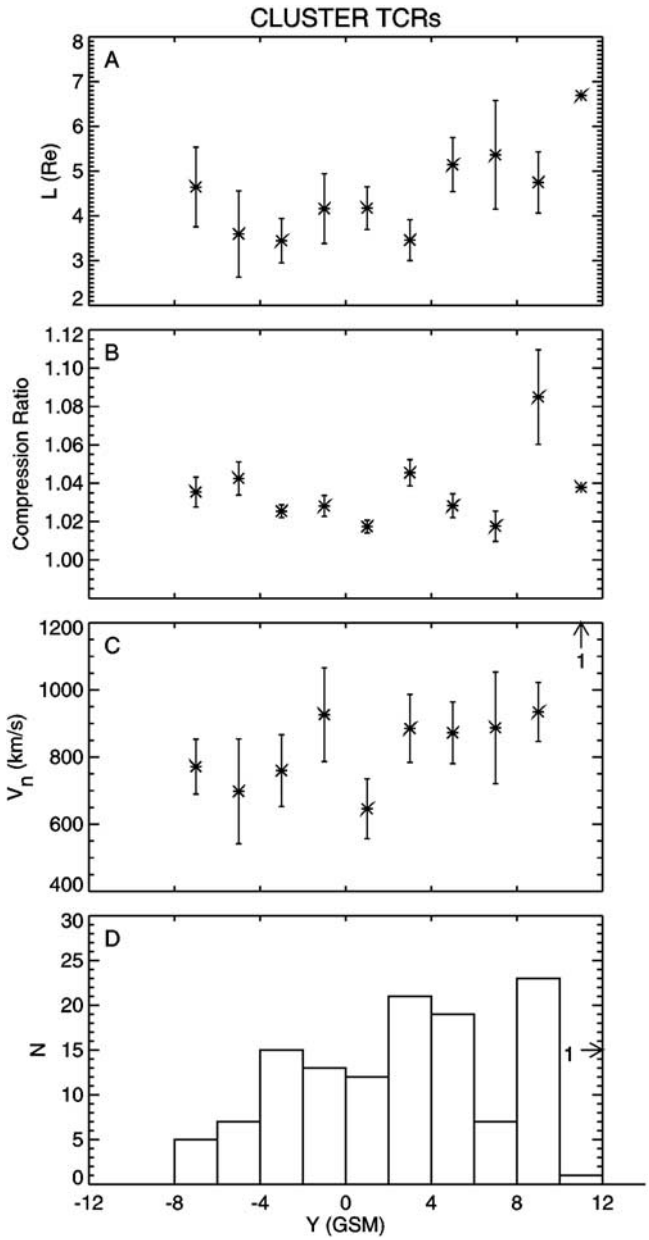

Figure 5b. Mean values of TCR thickness, compression ratio, propagation speed and number of events as a function of GSM *Y*. The error bars provided are standard errors in the mean for each bin. Note the broad duskside maximum in all of these quantities.

top part shows the inclination of the *B*3 direction relative to the GSM *XY* plane. The distribution is strongly peaked with a mean near the *XY* plane, i.e., $\langle \text{theta} \rangle = -2.5$ deg, indicating that the near-tail usually does not exhibit strong twisting as can occur at greater distances down the tail.

[20] However, the azimuthal orientation of the minimum variance direction, phi, measured relative to the $+Y$ axis showed a very broad distribution between ±70 deg. Although the mean value was near the $+Y$ direction, i.e., phi = −3.8 deg, the rather flat distribution indicates that *B*3 can lie far from the east-west direction. Finally, the angle between *B*3 and V_n was calculated for each event. Ideally, one would expect that these vectors would be 90 deg apart with the propagation direction normal to *B*3, which is itself perpendicular to the draping pattern. Indeed, this is the case with 90 deg being the peak bin of the histogram and a mean value for the $B3-V_n$ angle of

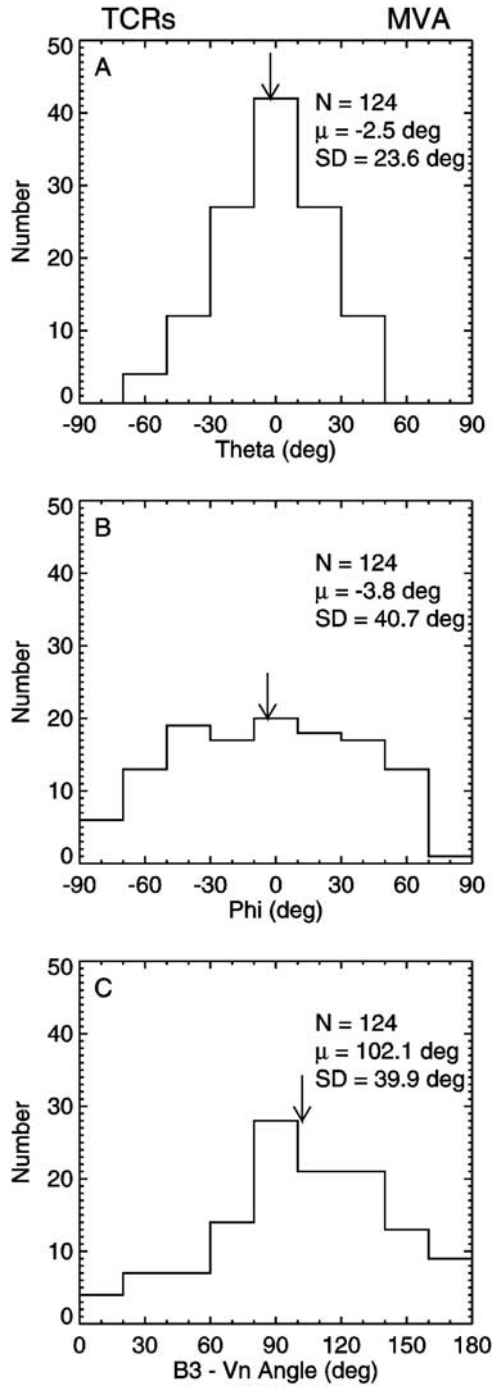

Figure 6. The inclination angles of the Cluster SN TCR minimum variance eigenvectors to the GSM *XY* plane are displayed in the top part. The azimuth angles for the minimum variance directions relative to the $+Y$ direction are shown in the second part. Finally, the angle between the TCR minimum variance direction and the propagation velocity is shown in the bottom part.

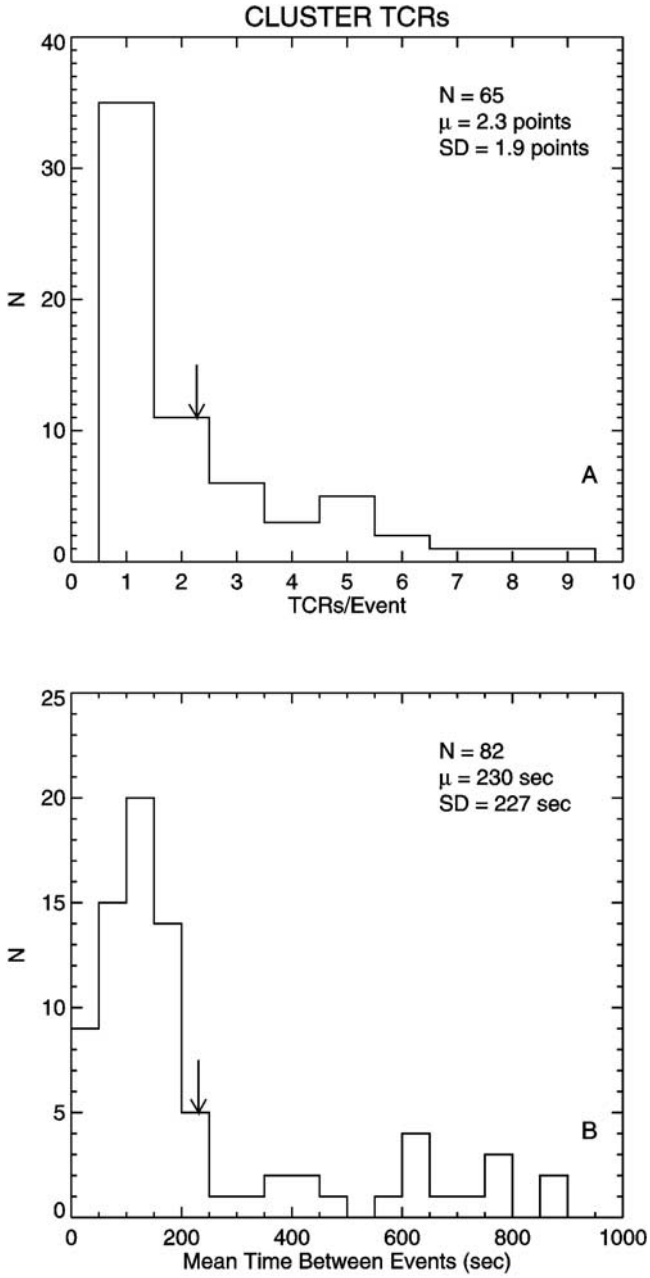

Figure 7. The top part displays a histogram of the number of TCRs per event. Multiple TCR events are defined as series of compression regions that are separated by less than 15 min. The lower part presents a histogram of the temporal spacing between TCRs within multiple TCR events.

102.1 deg. The closeness of this result to the expected 90 deg value demonstrates good consistency with the propagation direction derived from the Cluster measurements via triangularization.

5. Multiple TCR Events

[21] As in earlier studies of TCRs in the distant tail [*Slavin et al.*, 1993], we take compression regions that are separated in time by 15 min or less as being part of the same "event." Following this assumption, the top part of Figure 7 shows that 35 of the 148 total Cluster TCRs considered here are "single events" wherein the TCRs are separated by more than 15 min from any other TCRs. The number of "two TCR events" is 11, encompassing 22 TCRs, and so on. The largest number of TCRs found to occur without a break of more than 15 min is 9 and the mean number of TCRs per event is 2.3. Conversely, the bottom part of Figure 7 shows a histogram of the time interval between adjacent TCRs. The mode of the distribution is ~125 s, or about 2 min, but the mean separation is 230 s or just under 4 min. Accordingly, the temporal separations between TCRs are usually much longer than the typical duration, i.e., 35 s, of the individual compression regions.

[22] However, some multiple TCR events were observed in which the spacing between compression regions was similar to their durations. The 24 August 2001 interval shown in Figure 8 provides an example of a five TCR event. The durations of the individual compression regions is ~0.5 to 1 min, while the separations between the midpoints of the TCRs vary from ~1 to 2.5 min. Interestingly, the amplitude of the first TCR is the largest and the compression ratios of the later ones are smaller just as is commonly observed in the distant tail [*Slavin et al.*, 1993]. The reason for such a progression is not known. Multiple TCR events are potentially important because, as will be discussed later, they resemble the expected products of closed field line reconnection at multiple neutral lines with a periodic spacing. The flux ropes and their associated TCRs are then driven earthward, as in the 24 August 2001 event, or tailward when one of the X-lines begins to reconnect open flux tubes and develops into the NENL.

6. Substorm Association

[23] An example of very near-tail TCRs observed during a well-defined substorm on 17 September 2001 is shown in Figure 9. The bottom part displays the Kyoto Quick-Look *AL* index. Following a slow 30 min decrease, sometimes attributed to a "growth phase," there is a rapid onset to the expansion phase at 0738 UT and a broad negative bay between 0748 and 0800 UT. The recovery to preonset levels then takes about 1 hour.

[24] Nine TCRs are marked in Figure 9 with vertical lines. All of the TCRs exhibit the south-then-north ΔB_z variation associated with earthward propagation. Their motion is confirmed using the Cluster triangularization technique described earlier. The earthward propagation speeds determined in this manner is shown in the top part above each of the TCRs. Their speeds, ~800 to 1200 km/s, are comparable to the observed flow speeds measured for BBFs in the plasma sheet [*Nagai et al.*, 2000; *Angelopolous et al.*, 1992; *Baumjohann et al.*, 1990].

[25] The focus of this investigation is not the association of TCRs with substorms, but an initial examination has been carried out using superposed epoch analysis with the results displayed in Figure 10. Again, the midpoint of the TCR perturbation at s/c 1 is taken as the zero epoch and the SN and NS TCRs are analyzed separately. The analysis is limited to 2001 because the Kyoto Quick-Look *AL* is not yet available for 2002. The SN results mirror what was seen for 17 September 2001 substorm in the previous figure and the 19 September 2001 substorm examined by *Slavin et al.*

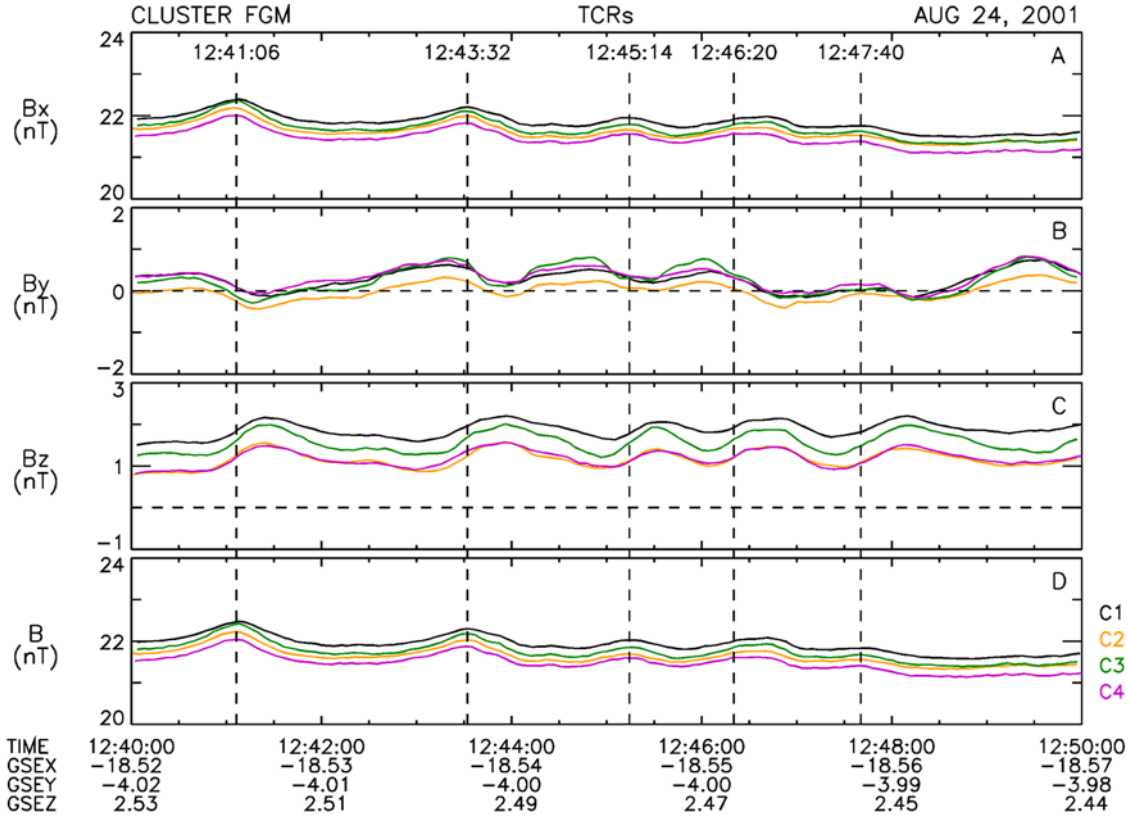

Figure 8. Example of a multiple SN TCR event observed on 24 October 2001.

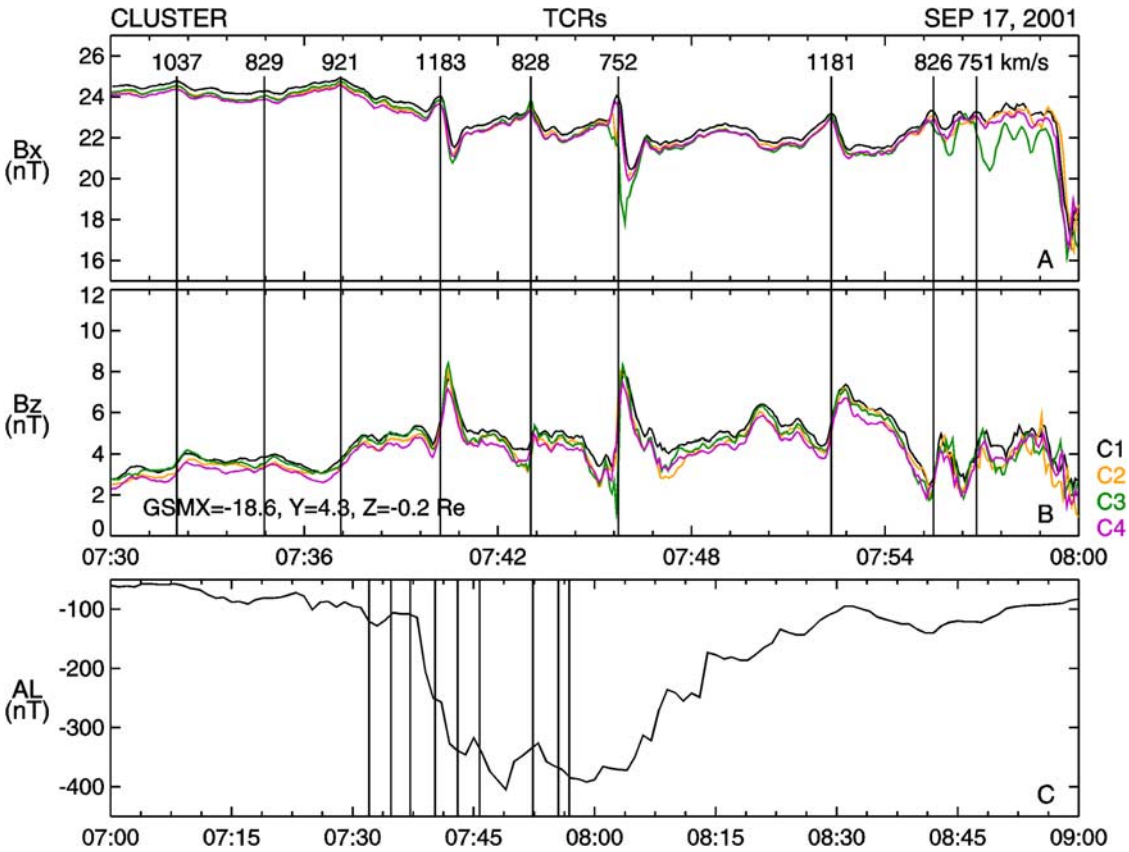

Figure 9. Example of TCRs observed by Cluster during a substorm on 17 September 2001. The propagation speed of the TCRs, all earthward, are shown at the top.

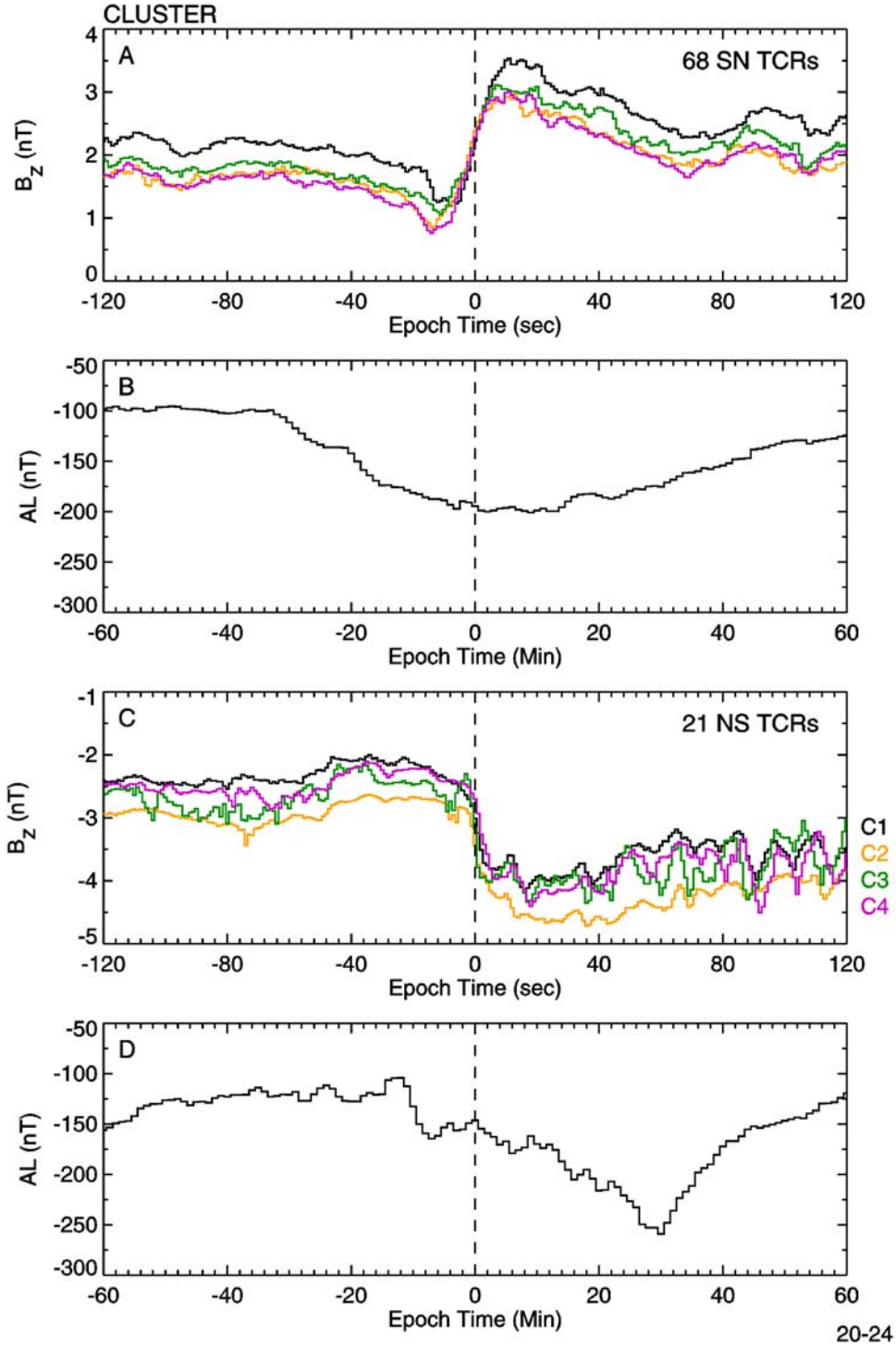

Figure 10. Superposed epoch analysis of the SN and NS TCRs and the Kyoto Quick-Look AL for 2001. Note, the zero epoch is the center point of the TCR signature measured by s/c 1 as in the previous figures.

[2003b]. To whit, the SN zero epoch corresponds to a broad negative bay in the AL index that begins ~35 min earlier and is still recovering 60 min later. These results suggest that SN TCRs occur during all phases of the substorm.

[26] The NS results in the bottom parts are somewhat different. There is an abrupt onset to the negative bay in *AL* about 10 min before the zero epoch and a narrow minimum 30 min after time zero. This result indicates that NS TCRs are generally seen very early in the substorm expansion phase and are rare later in substorms. Such a result is not surprising, as *X*-line formation is unlikely to take place very far earthward of the Cluster spacecraft and they are known to retreat tailward soon after formation [e.g., see *Ieda et al.*, 2001; *Slavin et al.*, 1993]. Accordingly, plasmoid-type flux

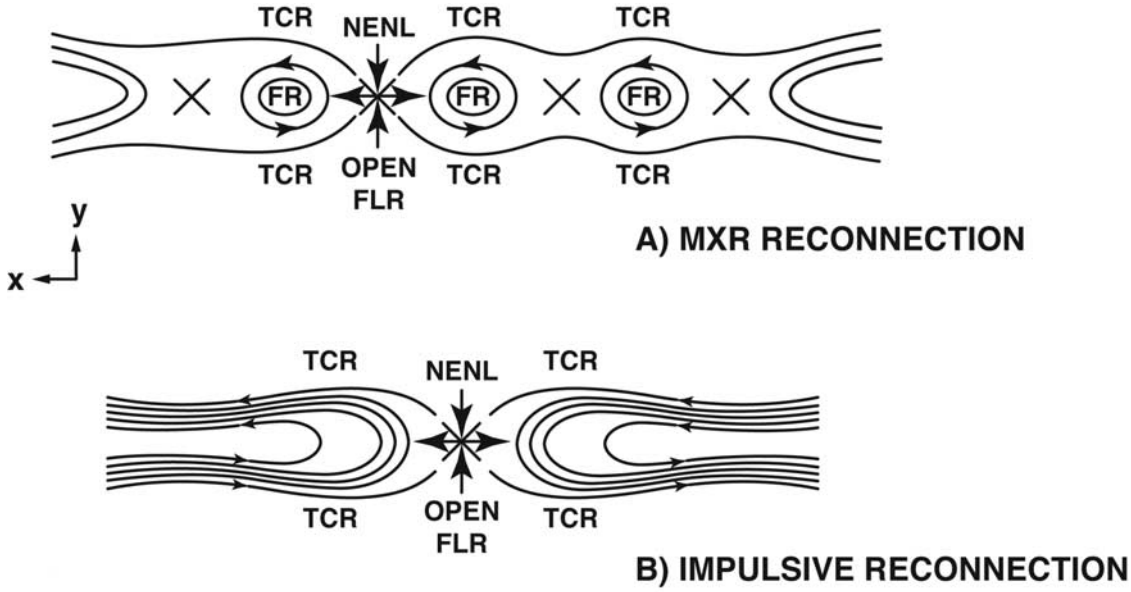

Figure 11. Schematic representations of two TCR generation mechanisms.

ropes and their associated NS TCRs generated by *X*-line formation earthward of Cluster would not have to move very far or for a very long time before being observed, as was found by our superposed epoch analysis.

7. Discussion

[27] In this study we have analyzed the traveling compression regions recently discovered in the near-tail in the Cluster measurements. These TCRs are important because they imply the presence of small, fast-moving bulges in the thickness of the plasma sheet that may provide an important source of information on the dynamics of the Earth's magnetotail. Toward this end it is especially important to determine the cause or causes of these TCR perturbations. Figure 11 depicts the two mechanisms that have been proposed for producing FTEs at the dayside magnetopause and TCRs in the near-tail; flux ropes [*Slavin et al.*, 2003c; *Moldwin and Hughes*, 1994; *Elphic et al.*, 1986; *Lee and Fu*, 1985] and impulsive reconnection [*Sergeev et al.*, 1992, 1987, submitted manuscript, 2005; *Southwood et al.*, 1988; *Biernat et al.*, 1987; V. S. Semenov et al., submitted manuscript, 2005].

[28] As diagrammed in the top part of the figure, small flux ropes may form due to reconnection at multiple *X*-lines. When reconnection takes place at two or more *X*-lines simultaneously it is termed "multiple *X*-line reconnection" or "MXR" reconnection [*Lee*, 1995; *Lee and Fu*, 1985]. Initially, reconnection in the plasma sheet involves only closed plasma sheet flux tubes. The Alfven speed is low at the center of the cross-tail current sheet so that the reconnection will proceed slowly and the outflow from the *X*-lines will be only ~100 km/s. However, as first noted by *Schindler* [1974], one of the *X*-lines will inevitably outpace the others in a nonlinear manner and begin to reconnect first flux tubes in the outer plasma sheet and, finally, lobe flux tubes where the Alfven speed is typically several thousand km/s [see *Hesse et al.*, 1996]. At that point, everything earthward of the first *X*-line to reconnect lobe flux tubes will be carried toward the Earth, and all material tailward of that point will be rapidly swept down the tail. Hence the formation of flux ropes by MXR reconnection is in a sense only a preliminary event to the open flux reconnection at a single neutral line in the NENL model of substorms [*Baker et al.*, 1996]. The existence of MXR reconnection is now supported by not only by numerical simulations [*Ohtani et al.*, 2004; *Shay et al.*, 2003], but also by the recent observation of a multiple *X*-line event by Geotail [*Deng et al.*, 2004].

[29] The bottom part of Figure 11 depicts the formation of TCRs due to "impulsive reconnection." As first suggested for the magnetopause by *Biernat et al.* [1987] and *Southwood et al.* [1988] and for the tail by *Sergeev et al.* [1987], intense "pulses" of reconnection might create "bulges" or "bubbles" in the current sheet about which the surrounding magnetic flux tubes drape and be compressed. These hot plasma bubbles are naturally ejected as a result of the fast flow out the *X*-line and the surrounding compression regions would accompany them. Sergeev et al. (submitted manuscript, 2005) and T. Penz et al. (submitted manuscript, 2005) have applied the impulsive tail reconnection model of Semenov et al. (submitted manuscript, 2005) to some of the TCRs observed by Cluster on 8 September 2002 and found good agreement between this model and the observations.

[30] Definitive testing of these two hypotheses will require multipoint measurements that provide simultaneous observations of the lobe compression region and the fast moving hot plasma bubble or flux rope in the central plasma sheet. Separations in the GSM *Z* direction of perhaps several times 10^4 km will be necessary which are not generally available at this time.

[31] We can, however, compare the predictions of the flux rope mechanism for near-tail TCR generation using the results of the Geotail flux rope studies carried out by *Slavin*

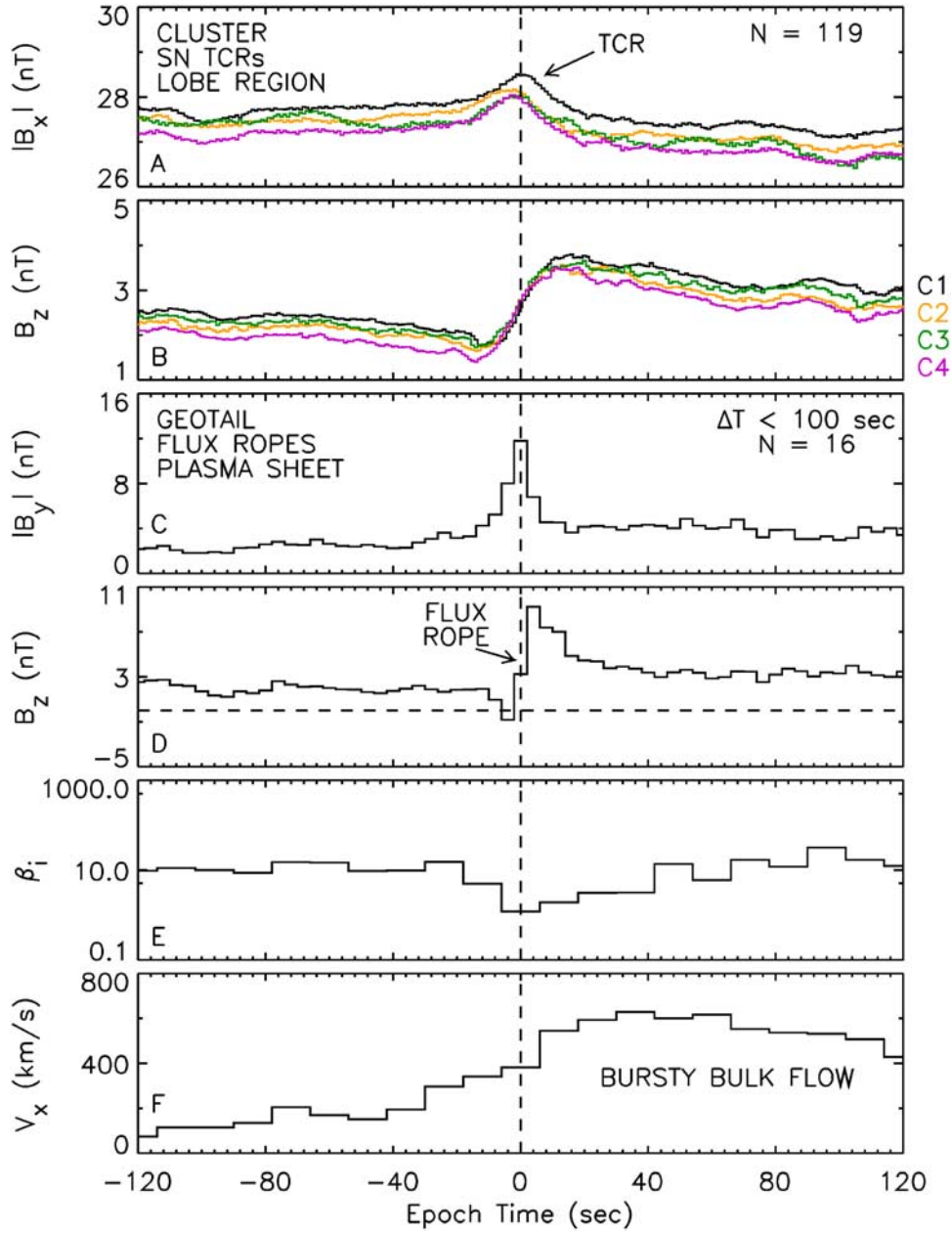

Figure 12a. Merged superposed epoch analyses of Cluster SN TCRs and Geotail bursty bulk flow (BBF)-type flux ropes (from *Slavin et al.* [2003a]).

et al. [2003a] using high time resolution magnetometer measurements. Toward this end, Figures 12a and 12b compare the Cluster TCRs measurements studied here and the Geotail magnetic flux ropes analyzed by *Slavin et al.* [2003a]. Superposed epoch analyses of the earthward and tailward propagating TCR and flux rope magnetic field signatures taken from this study and Figures 7 and 9 from *Slavin et al.* [2003a] have been combined to allow direct comparison. The B_x and B_z components of the Cluster magnetic fields are shown for the TCRs in the top two parts of both figures. The B_y and B_z components of the flux rope magnetic fields observed by Geotail are displayed in the middle two parts. Comparison of the traces shows that the duration of the near-tail TCRs and flux ropes are indeed comparable at ~30–40 s. The fact that TCR perturbations are just slightly broader than the flux ropes is consistent with this lobe field perturbation being due to the "draping" or "tenting" of the lobe flux tubes about a bulge in the plasma sheet. Finally, the plasma sheet ion beta ($\beta = nkT_i/B^2/2\mu_o$) and flow velocity are shown for the flux ropes, demonstrating that they are central plasma sheet, high beta ($\beta \sim 10$) structures associated with BBF-type flows.

[32] The orientations of the TCR minimum variance directions and the central axes of the near-tail flux ropes in the Geotail observations are examined in Figure 12c. Both the Cluster TCR minimum variance directions and the Geotail flux rope central axes tend to parallel the GSM *XY* plane with mean inclination angles of −2.6 deg and −3.4 deg, respectively. More remarkable are the wide

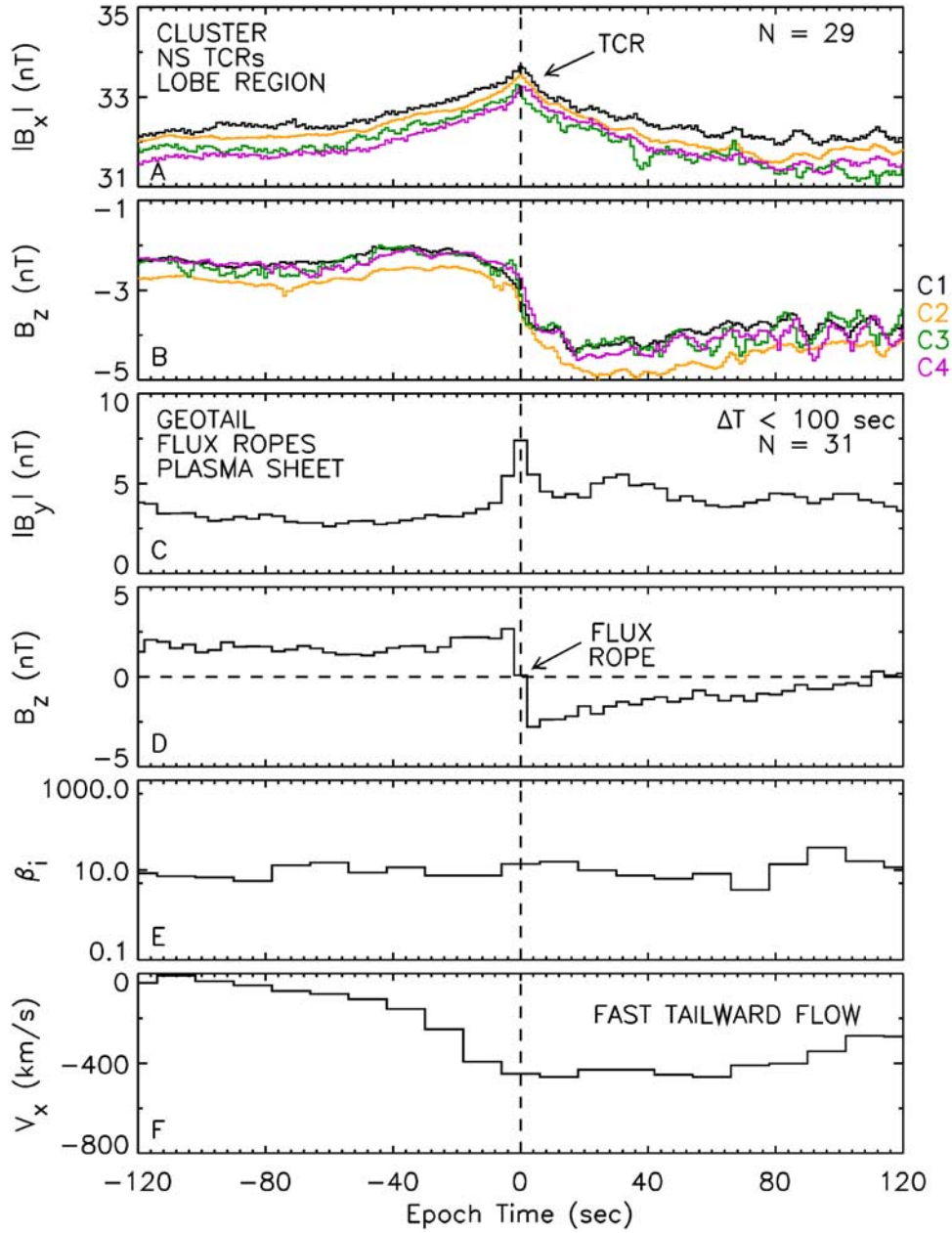

Figure 12b. Merged superposed epoch analyses of Cluster NS TCRs and Geotail Plasmid-type flux ropes (from *Slavin et al.* [2003a]).

range of azimuthal angles for the TCR minimum variance and flux rope central axes in the bottom two parts. While consistent with each other, the frequent, sometimes large, deviations of the central axes of the flux ropes, and their associated TCRs from the east-west direction are quite notable.

[33] *Hughes and Sibeck* [1987] speculated that asymmetries between the two ends of the flux rope magnetic fields in their connectivity to the geomagnetic field, or the interplanetary magnetic field in the magnetosheath, would result in unequal torques on the flux rope and skew it away from the east-west direction. However, the orientation of the flux ropes should also be influenced by the high-speed plasma sheet flows in which they are embedded. The wide range of orientations in the near-tail may then be due also to the limited east-west width of the BBF flows tending to shear and rotate the embedded flux ropes. In fact, new simulations by *Winglee* [2004] that include the effects of heavy ions on plasma sheet dynamics produce flux ropes that are highly skewed away from the east-west direction as a result of shear in the large-scale flow field due to differences in the rate of reconnection between the dawnside and duskside of the tail.

[34] Other significant results of our study concerns the asymmetries in TCR occurrence frequency and properties as function of east-west position in the tail and their substorm association. As shown in Figure 5b, TCRs are most likely to be observed on the duskside of the tail at $Y_{GSM} \sim 4$ to 8 R_E. Although less striking, the TCRs observed on the duskside of the tail also tend to be

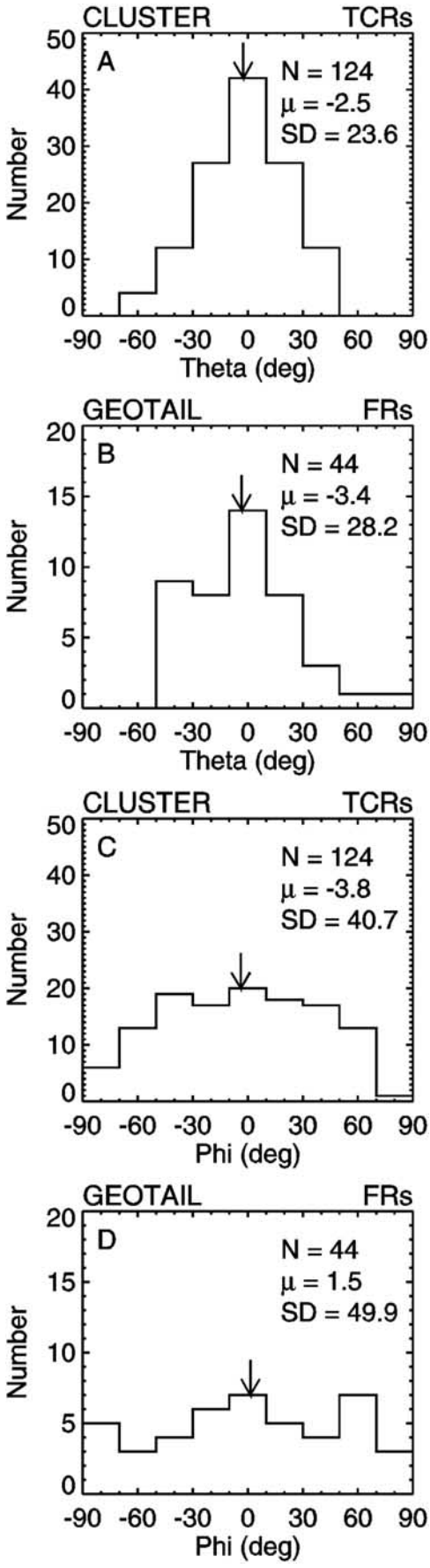

moving faster and to be larger in terms of their width. The Geotail results of *Slavin et al.* [2003a] are used, again, in Figure 12d to compare the dawn-dusk asymmetries found in the Cluster TCR observations with flux ropes in the near-tail plasma sheet. The tendency for larger widths, L, on the duskside of the tail is actually stronger in the flux ropes than in the TCRs, as shown in parts A and B. Averaged over of all events, the mean TCR width is 4.3 R_E, as compared with a mean flux rope diameter of 2.9 R_E. The flux rope speeds, in contrast, exhibit less dawn-dusk asymmetry than the TCRs (see parts C and D). In addition, the flux rope speeds are somewhat slower than typical BBFs and the TCRs.

[35] The reasons for this difference in TCR and flux rope speed are unclear. It may be an artifact of the flux rope selection criteria used by *Slavin et al.* [2003a]. The purpose was to select and analyze flux ropes that were quasi-force free, i.e., they were required to have strong core fields. Since it probably takes time for flux ropes to evolve toward this lower energy state, it may be that the *Slavin et al.* [2003a] flux ropes tended to be associated with intervals of slower than typical BBF flows. However, the reason for the speed differences between the flux rope and TCR observations could also be due to changes in the upstream solar wind between the 1998–1999 epoch of the Geotail flux rope observations [*Slavin et al.*, 2003a] and the 2001–2002 Cluster TCR measurements used in this study. Still, it is remarkable that the asymmetries in the frequency of occurrence for TCRs and flux ropes in the bottom parts are so striking. A total of 16 and 28 flux ropes are observed for $Y < 0$ and $Y > 0$, respectively, as compared with 36 versus 88 TCR events.

[36] Studies of fast flows [*Nagai et al.*, 1998] and X-line occurrence [*Ueno et al.*, 1999] show dawn-dusk asymmetries similar to those of the Cluster TCRs, i.e., more frequent, intense events on the duskside of the plasma sheet as compared with the dawnside of the magnetotail. Theoretical studies of reconnection have shown that dawn-dusk asymmetries are expected even for uniform current sheets due to the differences in ion and electron motion on the kinetic level [*Karimbadi et al.*, 2004]. If, and how, such microscale effects manifest at the mesoscale and macroscale in flux ropes or high-speed flows is not known. Unfortunately, the uniformity of current sheet structure across the tail cannot be well determined using single spacecraft observations. Hence it remains to be learned whether the east-west asymmetries in tail dynamics are due to asymmetries in the initial conditions or the reconnection process itself.

[37] The Cluster TCRs are a factor of ~5 less frequent than for near-tail flux ropes in the Geotail data [*Slavin et al.*,

Figure 12c. The top part graphs the inclination angles of the Cluster TCR minimum variance eigenvectors. The second part plots the inclination angle for the central axes of the Geotail flux ropes modeled by *Slavin et al.* [2003a]. The azimuth angles for the TCR minimum variance eigenvectors and the flux rope central axes relative to the $+Y$ direction are shown in the third and fourth parts, respectively. Finally, a histogram of the angles between the TCR minimum variance directions and the propagation velocities is shown in the bottom part.

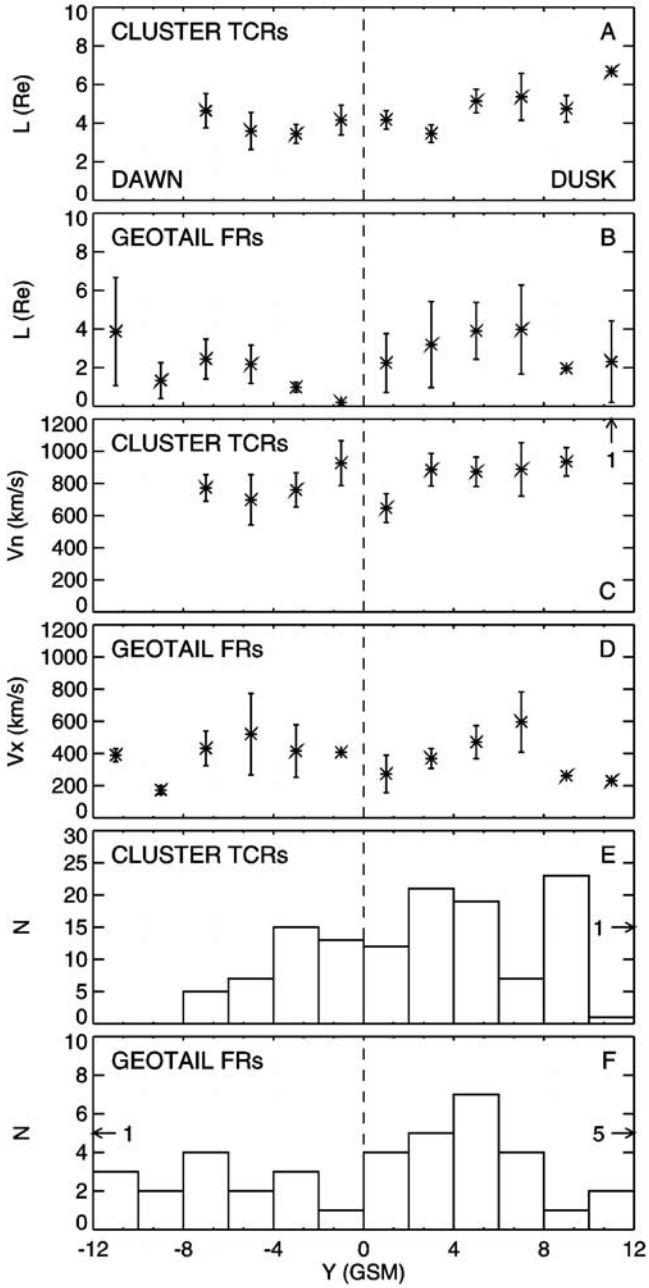

Figure 12d. Dawn-dusk asymmetries in Cluster TCR and Geotail flux rope length scales, L (parts A and C), TCR compression ratio (part B), speed (parts D and E) and frequencies of occurrence (parts F and G) are displayed.

2003a]. However, it is also possible that this difference in frequency of occurrence between the TCRs and flux ropes is primarily due to the low apogee of the Cluster orbit, 20 R_E, as compared with the 30 R_E apogee of Geotail or differences in event selection criteria and sensitivity. Of the flux ropes observed by Geotail a little more than half were moving tailward and would not be expected to be observed closer to the Earth. Comparing the frequency of occurrence of earthward propagating TCRs to earthward moving flux ropes reduces the discrepancy to a factor of ~2.5. In addition, the strength of the lobe field increases as distance from the Earth decreases. The efficiency with which TCRs can be identified is expected to decrease as the relative amplitude of the TCRs, $\Delta B/B$, becomes smaller and the signal-to-noise ratio for their detection worsens. In contrast, both TCRs and plasmoid-type flux ropes are readily observable in the more distant tail, where the background lobe field is weak, and can often be mapped to substorms on one-to-one or many-to-one basis [see *Huang et al.*, 2003; *Ieda et al.*, 2001; *Slavin et al.*, 1992]. The flux ropes carried earthward by BBF flows may also quickly dissipate through "re-reconnection" with the increasingly strong dipolar magnetic fields they encounter as they move earthward (see discussion in the work of *Slavin et al.* [2003a]). Accordingly, the uncertainties surrounding the temporal evolution and frequencies of occurrence for near-tail flux ropes and TCRs are such that the flux rope model can explain a major fraction of the TCRs in the Cluster observations, but it is not possible to determine with any certainty the magnitude of the remaining fraction that may be due to impulsive reconnection.

[38] Concerning where the NENL forms, our results indicate that the ratio of earthward to tailward TCRs observed by Cluster at $X \sim -18$ R_E (see distribution of events, Figure 5a) is about 4 to 1. This ratio is in close agreement with the recent Cluster survey of high-speed flows in the plasma sheet by *Nakamura et al.* [2004] that found ~22% of the flows were directed tailward. *Nagai et al.* [2000, 1998] used the Geotail measurements of fast plasma sheet flow to determine that the distance at which the occurrence of earthward and tailward flows become comparable is about $X \sim -25$ R_E. Similar results were also produced by *Ueno et al.* [1999] who examined the occurrence of reversals in V_x and B_z to identify encounters between Geotail and *X*-lines retreating tailward. Hence the available Cluster and Geotail observations appear to agree that when *X*-lines form in the tail they will be located at $X > -18$ R_E only about 20% of the time. Indeed, individual instances of NENL formation in the $X > -18$ R_E have been determined but only on a small number of occasions [e.g., *Slavin et al.*, 2002; *McPherron and Manka*, 1985].

[39] Detailed substorm analyses are beyond the scope of this study. However, the examples shown in Figures 2 and 9 and the superposed epoch analyses in Figure 10 leave little doubt that TCRs have a strong tendency to occur during substorms, especially during expansion phase. These results mirror the findings of previous studies of fast BBF flows in the plasma sheet. Although one-to-one mappings of individual high-speed flow events to specific substorms or auroral expansions are not always possible, case studies [e.g., *Huang et al.*, 2003; *Slavin et al.*, 2002; *Ieda et al.*, 1998; *McPherron and Manka*, 1985] and statistical analyses [e.g., *Nagai et al.*, 2000] show compelling associations that support close causal connections.

[40] Our results also provide clues as to the conditions that lead to NENL formation in the very near-tail, i.e., $X > -18$ R_E. The superposed epoch analyses in Figures 3b and 3c show that the very near-tail NENL formation necessary to produce NS TCRs occurs when the lobes are heavily loaded with excess magnetic flux. Specifically, our SN TCRs were observed when the mean lobe is ~27 nT while the NS events occurred during a mean lobe field of ~32 nT. MHD stress equilibrium considerations argue strongly that these large lobe magnetic field intensities lead to thinning of

the cross-tail current layer and the shifting of its location toward the Earth (e.g., M. M. Kuznetsova et al., submitted manuscript, 2005). Under such conditions it would be expected that reconnection would tend to occur closer to the Earth as our Cluster TCRs results indicate.

8. Summary

[41] In this study we have investigated the frequency of occurrence, physical properties, propagation characteristics, and substorm association of the traveling compression regions recently discovered in the Cluster observations. Our analyses have determined that the mean TCR duration in the near-tail is ~35 s, the average width is ~4 R_E, and their mean speed is 840 km/s. The TCR minimum variance directions were oriented largely in the GSM *XY* plane, but they displayed a wide range of orientations within that plane. The ~4 to 1 ratio of earthward to tailward propagating TCRs indicates that the NENL forms earthward of the Cluster spacecraft at X ~ −18 R_E, only about 20% of the time. Furthermore, a strong dawn-dusk asymmetry is observed, with more than twice as many TCRs being observed for $Y > 0$ as compared with $Y < 0$. The TCRs and flux ropes observed on the duskside of the tail are also larger and have higher propagation speeds. In addition, superposed epoch analysis using the Kyoto Quick-look *AL* index shows that the Cluster TCRs are substorm associated and tend to be observed during the expansion phase as is the case for most reconnection phenomena measured in the tail. Some examples of multiple TCR events were found to exhibit temporal separations on the order of the duration of the individual compression regions as expected for MXR reconnection events. However, the most probable separation observed during multi-TCR events was significantly larger at ~100–150 s. On the basis of the strong similarities between these TCR properties and those determined previously for magnetic flux ropes in the Geotail near-tail observations, we conclude that a large fraction of the TCRs in the Cluster observations are probably due to the rapid motion of small flux ropes in the plasma sheet. Impulsive reconnection may also play a significant role in the generation of compression regions, however, additional multipoint measurements and analysis will be necessary before its contribution is known.

[42] **Acknowledgments.** We thank T. Kamei and the Kyoto World Data Center for making the Quick Look Auroral Indices available over the internet. The expert assistance of C. Liebrecht with visualization and display of the Cluster measurements is gratefully acknowledged. Discussions with V. Sergeev, D. Fairfield, M. Kuznetsova, M. Goldstein, and D. Sibeck contributed significantly to this research project as did the sharing of prepublication manuscripts by V. Semenov and T. Penz. One of the authors, ET, was supported by the National Research Council Resident Research Associate Program. The work by KHG was financially supported by the Deutsches Zentrum fur Luft- und Raumfahrt DLR and the German Bundesministerium fur Bildung und Forschung under contract 50OC0103. Finally, the authors wish to express their appreciation to all of those who have contributed to the success of the Cluster mission.

[43] Lou-Chuang Lee thanks Jeffrey Hughes and Tsugunobu Nagai for their assistance in evaluating this paper.

References

Angelopolous, V., et al. (1992), Bursty bulk flows in the inner central plasma sheet, *J. Geophys. Res.*, *97*, 4027.

Baker, D. N., et al. (1987), Average plasma and magnetic field variations in the distant magnetotail associated with near-Earth substorm effects, *J. Geophys. Res.*, *92*, 71.

Baker, D. N., et al. (1996), Neutral line model of substorms: Past results and present view, *J. Geophys. Res.*, *101*, 12,975.

Balogh, A., et al. (1997), Cluster magnetic fields investigation, *Space Sci. Rev.*, *79*, 65.

Baumjohann, W., et al. (1990), Characteristics of high speed ion flows in the plasma sheet, *J. Geophys. Res.*, *95*, 3801.

Biernat, H. K., M. F. Heyn, and V. S. Semenov (1987), Unsteady Petschek reconnection, *J. Geophys. Res.*, *89*, 6689.

Birn, J., M. Hesse, and K. Schindler (1989), Filamentary structure of a three-dimensional plasmoid, *J. Geophys. Res.*, *94*, 241.

Deng, X. H., et al. (2004), Geotail encounter with reconnection diffusion in the Earth's magnetotail: Evidence of multiple X-line collisionless reconnection?, *J. Geophys. Res.*, *109*, A05206, doi:10.1029/2003JA010031.

Elphic, R. C., et al. (1986), ISEE 1 and 2 observations of magnetic flux ropes in the magnetotail: FTEs in the plasma sheet?, *Geophys. Res. Lett.*, *14*, 648.

Hesse, M., et al. (1996), MHD simulations of the transition of magnetic reconnection from closed to open field lines, *J. Geophys. Res.*, *101*, 10,805.

Hones, E. W., Jr. (1977), Substorm processes in the magnetotail: Comments on "On hot tenuous plasma, fireballs, and boundary layers in the Earth's magnetotail" by L. A. Frank et al., *J. Geophys. Res.*, *82*, 5633.

Hones, E. W., Jr., et al. (1984), Structure of the magnetotail at 220 R_e and its response to geomagnetic activity, *Geophys. Res. Lett.*, *11*, 5.

Huang, C.-S., et al. (2003), Periodic magnetospheric substorms: Multiple space-based and ground-based observations, *J. Geophys. Res.*, *108*(A11), 1411, doi:10.1029/2003JA009992.

Hughes, W. J., and D. G. Sibeck (1987), On the three dimensional structure of plasmoids, *Geophys. Res. Lett.*, *14*, 636.

Ieda, A., et al. (1998), Statistical analysis of plasmoid evolution with GEOTAIL observations, *J. Geophys. Res.*, *103*, 4435.

Ieda, A., et al. (2001), Plasmoid ejection and auroral brightenings, *J. Geophys. Res.*, *106*, 3845.

Karimabadi, H., D. Krauss-Varban, J. D. Huba, and H. X. Vu (2004), On magnetic reconnection regimes and associated asymmetries: Hybrid, Hall-less hybrid, and Hall-MHD simulations, *J. Geophys. Res.*, *109*, A09205, doi:10.1029/2004JA010478.

Lee, L. C. (1995), A review of magnetic reconnection: MHD models, in *Physics of the Magnetopause*, *Geophys. Monogr. Ser.*, vol. 90, edited by P. Song, B. U. O. Sonnerup, and M. F. Thomsen, pp. 139–153, AGU, Washington, D.C.

Lee, L. C., and Z. F. Fu (1985), A theory of magnetic flux transfer at the Earth's magnetopause, *Geophys. Res. Lett.*, *12*, 105.

Machida, S., et al. (2000), Statistical visualization of the Earth's magnetotail during substorms by means of multidimensional superposed epoch analysis with Geotail data, *J. Geophys. Res.*, *105*, 25,291.

McPherron, R. L., and R. H. Manka (1985), Dynamics of the 10:54 UT, March 22, 1979 substorm, *J. Geophys. Res.*, *90*, 1175.

Moldwin, M. B., and W. J. Hughes (1991), Plasmoids as flux ropes, *J. Geophys. Res.*, *96*, 14,051.

Moldwin, M. B., and W. J. Hughes (1992), On the formation and evolution of plasmoids: A survey of ISEE 3 Geotail data, *J. Geophys. Res.*, *97*, 19,259.

Moldwin, M. B., and W. J. Hughes (1994), Observations of Earthward and tailward propagating flux rope plasmoids: Expanding the plasmoid model of geomagnetic substorms, *J. Geophys.Res.*, *99*, 183.

Mukai, T., et al. (1996), Structure and kinetic properties of plasmoids and their boundary regions, *J. Geomagn. Geolectr.*, *48*, 541.

Mukai, T., et al. (1998), Dynamics and kinetic properties of plasmoids and flux ropes: Geotail observations, in *New Perspectives on the Earth's Magnetotail*, *Geophys. Monogr. Ser.*, vol. 105, edited by A. Nishida, D. N. Baker, and S. W. H. Cowley, pp. 117–132, AGU, Washington, D.C.

Nagai, T., et al. (1994), Initial Geotail survey of magnetic substorm signatures in the magnetotail, *Geophys. Res. Lett.*, *21*, 2991.

Nagai, T., et al. (1998), Structure and Dynamics of magnetic reconnection for substorm onsets with GEOTAIL observations, *J. Geophys. Res.*, *103*, 4419.

Nagai, T., et al. (2000), Development of substorms in the near-Earth tail, *Adv. Space Res.*, *25*, 1651.

Nakamura, R., et al. (2004), Spatial scale of high-speed flows in the plasma sheet observed by Cluster, *Geophys. Res. Lett.*, *31*, L09804, doi:10.1029/2004GL019558.

Ohtani, S.-I., M. A. Shay, and T. Mukai (2004), Temporal structure of the fast convective flow in the plasma sheet: Comparison between

observations and two-fluid simulations, *J. Geophys. Res.*, *109*, A03210, doi:10.1029/2003JA010002.
Owen, C. J., and J. A. Slavin (1992), Energetic ion events associated with traveling compression regions, *Proceedings of International Conference on Substorms, ESA SP-335*, pp. 365–370, Eur. Space Agency. Paris.
Owen, C. J., J. A. Slavin, A. N. Fazakerley, M. W. Dunlop, and A. Balogh (2005), Cluster electron measurements of the separatrix layer during traveling compression regions, *Geophys. Res. Lett.*, *32*, L03104, doi:10.1029/2004GL021767.
Richardson, I. G., et al. (1987), Plasmoid-associated energetic ion bursts in the deep geomagnetic tail: Properties of plasmoids and the post-plasmoid plasma sheet, *J. Geophys. Res.*, *92*, 9997.
Russell, C. T., and R. C. Elphic (1978), Initial ISEE magnetometer results: Magnetopause observations, *Space Sci. Rev.*, *22*, 681.
Schindler, K. (1974), A theory of the substorm mechanism, *J. Geophys. Res.*, *79*, 2803.
Sergeev, V. A., V. S. Semenov, and M. V. Sidneva (1987), Impulsive reconnection in the magnetotail during substorm expansion, Current sheet thickness in the near-Earth plasma sheet during substorm growth phase, *Planet. Space Sci.*, *35*, 1199.
Sergeev, V. A., et al. (1992), A two-satellite study of nightside flux transfer events in the plasma sheet, *Planet. Space Sci.*, *40*, 1551.
Shay, M. A., et al. (2003), Inherently three dimensional magnetic reconnection: A mechanism for bursty bulk flows?, *Geophys. Res. Lett.*, *30*(6), 1345, doi:10.1029/2002GL016267.
Shirai, H., et al. (2001), Enhancements of lobe ion density and velocity associated with plasmoids, *J. Geophys. Res.*, *106*, 29,935.
Slavin, J. A., et al. (1984), Substorm associated traveling compression regions in the distant tail: ISEE-3 geotail observations, *Geophys. Res. Lett.*, *11*, 657.
Slavin, J. A., et al. (1989), CDAW-8 observations of plasmoid signatures in the geomagnetic tail: An assessment, *J. Geophys. Res.*, *94*, 15,153.
Slavin, J. A., et al. (1992), ISEE-3 Plasmoid and TCR Observations during an extended interval of substorm activity, *Geophys. Res. Lett.*, *19*, 825.
Slavin, J. A., et al. (1993), ISEE-3 observations of traveling compression regions in the Earth's magnetotail, *J. Geophys. Res.*, *98*, 15,425.
Slavin, J. A., et al. (1998), ISTP observations of plasmoid ejection: IMP 8 and Geotail, *J. Geophys. Res.*, *103*, 119.
Slavin, J. A., et al. (2002), Simultaneous observations of Earthward flow bursts and plasmoid ejection during magnetospheric substorms, *J. Geophys. Res.*, *107*(A7), 1106, doi:10.1029/2000JA003501.
Slavin, J. A., et al. (2003a), Geotail observations of magnetic flux ropes in the plasma sheet, *J. Geophys. Res.*, *108*(A1), 1015, doi:10.1029/2002JA009557.
Slavin, J. A., et al. (2003b), Cluster measurements of electric current density within a flux rope in the plasma sheet, *Geophys. Res. Lett.*, *30*(7), 1362, doi:10.1029/2002GL016411.
Slavin, J. A., et al. (2003c), Cluster four spacecraft measurements of small traveling compression regions in the near-tail, *Geophys. Res. Lett.*, *30*(23), 2208, doi:10.1029/2003GL018438.
Sonnerup, B. U. O., and L. J. Cahill (1967), Magnetopause structure and attitude from Explorer 12 observations, *J. Geophys. Res.*, *72*, 171.
Sonnerup, B. U. O., H. Hasegawa, and G. Paschmann (2004), Anatomy of a flux transfer event seen by Cluster, *Geophys. Res. Lett.*, *31*, L11803, doi:10.1029/2004GL020134.
Southwood, D. J., C. J. Farrugia, and M. A. Saunders (1988), What are flux transfer events?, *Planet. Space Sci.*, *36*, 503.
Taguchi, S., et al. (1997), Temporal relationship between mid-tail TCRs and substorm onset: Evidence for near-Earth neutral line formation in the late growth phase, *J. Geophys. Res.*, *103*, 26,607.
Taguchi, S., J. A. Slavin, and R. P. Lepping (1998), Traveling compression regions in the mid-tail: 15 years of IMP 8 observations, *J. Geophys. Res.*, *103*, 17,641.
Ueno, G., et al. (1999), Distribution of X-type magnetic neutral lines in the magnetotail with Geotail observations, *Geophys. Res.*, *26*, 3341.
Winglee, R. M. (2004), Ion cyclotron and heavy ion effects in a global magnetotail, *J. Geophys. Res.*, *109*, A09206, doi:10.1029/2004JA010385.
Zong, Q.-G., et al. (2004), Cluster observations of earthward flowing plasmoid in the tail, *Geophys. Res. Lett.*, *31*, L18803, doi:10.1029/2004GL020692.

A. Balogh, S. Imber, and E. A. Lucek, Space and Atmospheric Physics, Imperial College, London, W72BZ, UK.
M. W. Dunlop, Rutherford Appleton Laboratory, Chilton, Didcot, Oxfordshire, OX11, 0QX, UK.
K.-H. Glassmeier, Institut für Geophysik und extraterrestrische Physik, Technische Universat Braunschweig, D-38106 Braunschweig, Germany.
M. Hesse, J. A. Slavin, and E. I. Tanskanen, Laboratory for Extraterrestrial Physics, NASA Goddard Space Flight Center, Greenbelt, MD 20771, USA. (jslavin@pop600.gsfc.nasa.gov)
C. J. Owen, Mullard Space Science Laboratory, University College London, Holmbury St. Mary, Dorking, Surrey, RH5 6NT, UK.